(12) INTERNATIONAL APPLICATION PUBLISHED UNDER THE PATENT COOPERATION TREATY (PCT)

(19) World Intellectual Property Organization
International Bureau

(43) International Publication Date
12 September 2014 (12.09.2014)

WIPO | PCT

(10) International Publication Number
WO 2014/138367 A1

(51) International Patent Classification:
A61K 31/513 (2006.01) *A61K 31/52* (2006.01)

(21) International Application Number:
PCT/US2014/021129

(22) International Filing Date:
6 March 2014 (06.03.2014)

(25) Filing Language: English

(26) Publication Language: English

(30) Priority Data:
61/773,296 6 March 2013 (06.03.2013) US

(71) Applicant: **BRANDEIS UNIVERSITY** [US/US]; 415 South Street, Waltham, MA 02453-2728 (US).

(72) Inventors: **XU, Bing**; 46 Collins Road, Newton, MA 02468 (US). **YI, Kuang**; 295 Crescent Street, Waltham, MA 02453 (US).

(74) Agents: **GORDON, Dana M.** et al.; Foley Hoag LLP, Patent Group, 155 Seaport Blvd., Boston, MA 02210-2600 (US).

(81) Designated States *(unless otherwise indicated, for every kind of national protection available)*: AE, AG, AL, AM, AO, AT, AU, AZ, BA, BB, BG, BH, BN, BR, BW, BY, BZ, CA, CH, CL, CN, CO, CR, CU, CZ, DE, DK, DM, DO, DZ, EC, EE, EG, ES, FI, GB, GD, GE, GH, GM, GT, HN, HR, HU, ID, IL, IN, IR, IS, JP, KE, KG, KN, KP, KR, KZ, LA, LC, LK, LR, LS, LT, LU, LY, MA, MD, ME, MG, MK, MN, MW, MX, MY, MZ, NA, NG, NI, NO, NZ, OM, PA, PE, PG, PH, PL, PT, QA, RO, RS, RU, RW, SA, SC, SD, SE, SG, SK, SL, SM, ST, SV, SY, TH, TJ, TM, TN, TR, TT, TZ, UA, UG, US, UZ, VC, VN, ZA, ZM, ZW.

(84) Designated States *(unless otherwise indicated, for every kind of regional protection available)*: ARIPO (BW, GH, GM, KE, LR, LS, MW, MZ, NA, RW, SD, SL, SZ, TZ, UG, ZM, ZW), Eurasian (AM, AZ, BY, KG, KZ, RU, TJ, TM), European (AL, AT, BE, BG, CH, CY, CZ, DE, DK, EE, ES, FI, FR, GB, GR, HR, HU, IE, IS, IT, LT, LU, LV, MC, MK, MT, NL, NO, PL, PT, RO, RS, SE, SI, SK, SM, TR), OAPI (BF, BJ, CF, CG, CI, CM, GA, GN, GQ, GW, KM, ML, MR, NE, SN, TD, TG).

Published:

— *with international search report (Art. 21(3))*

WO 2014/138367 A1

(54) Title: INHIBITION OF TUMOR GROWTH WITH AGGREGATES OF SMALL MOLECULES

(57) Abstract: Disclosed herein are fibrillar molecular aggregates, which are morphologically and phenotypically similar to oligomers of aberrant proteins. The molecular aggregates, formed by self-assembly of small hydrophobic molecules, prevent the growth of microtubules. This unprecedented mechanism of "self-assembly to interfere with self-organization" allows inhibition of the growth of cancer cells.

Inhibition of Tumor Growth with Aggregates of Small Molecules

RELATED APPLICATIONS

This application claims the benefit of priority to United States Provisional Patent Application serial number 61/773,296, filed March 6, 2013; the contents of which are hereby incorporated by reference.

GOVERNMENT SUPPORT

This invention was made with government support under R01-CA142746 awarded by the National Institutes of Health. The government has certain rights in the invention.

BACKGROUND OF THE INVENTION

Cancer and Alzheimer's disease are major threats to the public health. While both diseases are still being understood, epidemiological and clinical studies suggest that there is an inverse association between cancer and Alzheimer's disease. The intriguing inverse association has stimulated the hope that the understanding of the mechanisms underlying the inverse association may lead to novel therapies for both diseases. Several plausible biological mechanisms have been postulated. For example, several groups have suggested that cancer and Alzheimer's disease may share same genes (e.g., TP53 and PIN1) and biological pathways (e.g., Wnt) related to activation and deregulation of the cell cycle. While the genetic links between cancer and Alzheimer's disease are biological plausibility that contributes to the observed inverse comorbidity, the complexity of the two groups of diseases obviously is beyond genetic definition, suggesting that other processes and mechanisms deserve serious consideration and rigorous examination.

In fact, after long debates about the causative agents of Alzheimer's disease, now it is suggested that amyloid oligomers are the most neurotoxic species. Recent studies also suggest that the early aggregates of misfolded non-disease-associated proteins and oligomers of disease-associated proteins (e.g., Aβs) exhibit similar inherent cytotoxicity, an important mechanistic advance that implies a common mechanism of the cytotoxicity of the aggregates. Since the aggregation of proteins (especially aberrant proteins), which represents a kinetically trapped state, is not directly defined at the genetic level, the elucidation of the molecular mechanism of the cytotoxicity of the aggregates may provide new information that eludes genetic studies. Despite its potential significance, the common origin of the cytotoxicity of the aggregates of aberrant proteins remains to be established.

SUMMARY OF THE INVENTION

In certain embodiments, the invention relates to a method of treating or preventing cancer comprising the step of

administering to a subject in need thereof a plurality of hydrophobic, self-assembling monomers.

In certain embodiments, the invention relates to a method of retarding or preventing the growth of a microtubule comprising the step of

contacting tubulin with a plurality of hydrophobic, self-assembling monomers.

In certain embodiments, the invention relates to any one of the aforementioned methods, wherein the hydrophobic, self-assembling monomer is represented by **Formula I**:

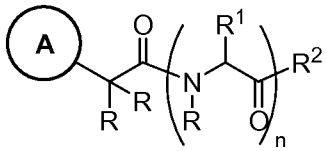

I

wherein, independently for each occurrence,

 is aryl, heteroaryl, aralkyl, or heteroaralkyl;

R is H or alkyl;

R^1 is aralkyl or heteroaralkyl;

R^2 is H, alkyl, -OR, or $-NR_2$;

n is 1, 2, 3, 4, 5, 6, 7, 8, 9, 10, 11, 12, 13, 14, 15, 16, 17, 18, 19, or 20.

BRIEF DESCRIPTION OF THE FIGURES

Figure 1 depicts characteristics of fibrillar aggregates of **1**. (a) Negative-stained TEM images of the solution of **1** at 400 μM and (b) the histogram of the length distribution of fibrillar aggregates according to the TEM images of **1** at 400 μM. (c) The plot of the heat release, measured by ITC, from the dilution of the solution of **1** at different concentrations. Data are presented as mean ± SD. (d) Circular dichroism (CD) spectra of **1** at different concentrations. (e) ThT fluorescence emission at 480 nm (λ_{ex} 440 nm) of ThT (20 μM) with increased concentrations of **1** in PBS buffer. See also Figure 8.

Figure 2 depicts the cytotoxicity of **1**. Cell viability assay (MTT) of HeLa cells after 24 and 48 h of treatment with (a) as prepared or (b) filtered medium containing different concentrations of **1**. Also shown are MTT assays of **1** towards (c) MC-7, (d) HepG2, (e) T98G and (f) PC12 cell lines. Data are presented as mean ± SD of three

independent experiments. (g) Tumor progression curves of mice bearing HeLa tumors. 0.1 mL of **1** at 5 mM or 0.5 mM in PBS buffers or just PBS buffer as control (six doses, starting day 1) was subcutaneous peritumorally injected every three days. Data are presented as mean ± SD of relative tumor volume (n = 4 for treatment groups and n = 3 for control group). $*p < 0.05$, by Student's t test. (at day 19, 5 mM = bottom data point; 0.5 mM = middle data point; control = top data point). (h) A representative image to show the mice, started with similar initial tumor volume (V_0), from each group on 19^{th} day of treatment. White arrows point at tumor. See also Figure 9, Figure 10, and Figure 11.

Figure 3 depicts the response of cancer cells toward molecular aggregates of **1**. (a) Intracellular concentration of **1** in HeLa cells treated with **1** for 12 h at different temperatures measure by LC-MS (left bar = 37 °C; right bar = 4 °C). (b) Confocal images of FITC annexin V and PI stained HeLa cells without incubation with **1** (live cells), HeLa cells treated with 400 μM of **1** for 36 h, and necrotic HeLa cells (induced by DMSO). Scale bar = 20 μm. (c) Fluorescence emission of 7-AAD and **1** in cell lysate (15,000 cell/mL) at λ_{ex} = 488 nm. (d) Cell cycle analysis, by flow cytometry, of HeLa cells treated with 0, 300 or 400 μM of **1** for 24 h. Depletion of G2/M phase occurs in cells treated with 400 μM of **1**. (e) Cell migration assay of HeLa cells treated with 0, 300, 400 or 500 μM of **1**. The gaps were created on the HeLa cells of 100% confluence in 24 well plates, and measured after incubation for 18 h.

Figure 4 depicts a hydrogel based protein pull-down assay. Collected samples are: complete cell lysate (C), unbound protein (U), wash-off proteins (W1, W2 and W3), proteins that bound specifically with hydrogel (B) and hydrogel itself as background (H). After SDSPAGE, the protein constituent of each sample was analyzed by silver stain, Coomassie stain, and the identity of the cytoskeletal proteins was further confirmed by Western blot.

Figure 5 depicts *in vitro* and cell-based assays demonstrating the interaction between tubulin and molecular aggregates of **1**. Tubulin polymerization assay in the presence of **1**. *In vitro* tubulin polymerization reactions in (a) as prepared or (c) filtered reaction cocktail without **1** (control) or with different concentrations of **1**. The amount of microtubule is in proportion to optical density at 340 nm. The calculated polymerization rate (V_{max}) and the final tubulin polymer mass *vs* concentrations of **1** from tubulin polymerization in (b) as prepared or (d) filtered reaction cocktail. Negative stained TEM images of molecular aggregates of **1** binding with tubulin. (e) Buffer (control) or **1** (final

concentration at 200 to 500 μM) was introduced into reaction cocktail containing fully assembled microtubule (after 60 min of polymerization). The amount of microtubule remain unchanged after 30 min. (f) Molecular aggregates of **1** (400 μM) incubated with tubulins heterodimers in general tubulin buffer. Scale bar = 40 nm. White arrows point at tubulin clusters on the molecular aggregates of **1**. Confocal images of tubulin stained HeLa and other cell lines. (g) Time dependent cytotoxicity of **1** towards HeLa cells. Data are presented as mean ± SD of three independent experiments. Tubulin staining of HeLa cells treated with as-prepared medium containing (h) 0 μM, (i) 200 μM, (j) 300 μM and (k) 400 μM of **1**, and filtered medium (l) containing 400 μM of **1** for 24 h. Insets are 3X enlarged images. T98G (m, n) and PC12 (o, p) were also treated with as-prepared medium containing 0 or 400 μM of **1** for 24 h for tubulin staining. DNA was counterstained blue by DAPI. Scale bar = 10 μm. See also Figure 12.

Figure 6 is an illustration of the interaction between molecular aggregates of **1** and tubulin heterodimers inside cells. Molecules of **1** self-assemble to form cross-β structure that results in fibrillar molecular aggregates (structural simulation showing in gray) in aqueous medium. The molecular aggregates of **1** cluster and disorient short microtubules on the surface, and consequently prevent the formation of oriented long microtubule fibrils. Red arrows point out the orientation of each microtubule.

Figure 7 is an illustration of a plausible molecular mechanism of selective cytotoxicity induced by **1**. Due to the Warburg effect, cancer cells uptake an excessive amount of **1** by active transportation. **1** is accumulated in cancer cells, and its aggregates inhibit growth of microtubule, which eventually triggers the apoptosis cascade. In neuronal cells, the uptake and accumulation of **1** is slower than in cancer cells, resulting in less aggregates of **1**. The presence of abundant microtubule-stabilizing proteins in the neuronal cells diminishes the inhibition of microtubule growth caused by the aggregates of **1**. Thus, **1** induces little acute cytotoxicity on neuronal cells.

Figure 8 depicts a TEM image of **1** at 300 μM. Related to Figure 1. Negative-stained TEM image of 1 at 300 μM in PBS buffer.

Figure 9 depicts the cytotoxicity of **1**. Related to Figure 2. (a) 72-h viability test of **1** on HeLa cells below threshold concentrations. Cytotoxicity of **1** towards other cancer cell lines (b) U87MG, (c) Capan-2 and (d) MES-SA. Data are presented as mean ± SD of three independent experiments.

Figure 10 depicts the long term cytotoxicity of **1** on PC12 cells. Related to Figure 2. (a) MTT viability test of cell incubated with gradient concentration of **1** for up to 7 days without changing medium. Data are presented as mean ± SD of three independent experiments. (b) Intracellular concentration of **1** in PC12 cells treated with **1** for 12 h at 37 °C measured by LC-MS (left bar = 400 μM; right bar = 300 μM). (c) Cells were subcultured and re-seeded with new medium containing the same concentration of **1** (0 for control group and 400 μM for test group) every 4 days. Data are presented as mean ± SD of three independent experiments.

Figure 11 depicts the effect of **1** on tumor progression in mice models bearing HeLa tumors. Related to Figure 2. (a) Body weight change curves of mice bearing HeLa tumors. Mice treated with 0.1 mL of 5 mM or 0.5 mM of **1** have no significant weight loss or weight gain comparing with mice in the control group. Data are presented as mean ± SD (n = 4 for treatment groups and n = 3 for control group) of relative tumor volume (at day 19, 5 mM = bottom data point; 0.5 mM = middle data point; control = top data point). Images showing mice bearing tumors from control group (b), 0.5 mM of **1** treatment group (c) and 5 mM of **1** treatment group (d) on 19th day of treatment. White arrows point at tumor.

Figure 12 depicts Negative stained TEM images of fibrillar aggregates of **1** binding with tubulin. Related to Figure 5. (a) Molecular aggregates of **1** incubated with biotinated tubulins then stained by streptavidin@Au in general tubulin buffer; (b) molecular aggregates of **1** alone stained by streptavidin@Au in general tubulin buffer; (c) anti-β-tubulin@Au stained fibrillar aggregates of **1** like structures in lysate of HeLa cells treated with 500 μM of **1** for 24 h. White arrow heads point at biotinated tubulin. Scale bar = 20 nm.

Figure 13 depicts CD spectra showing the polymorphic structures of nanofibers of **1**. (a) As **1** exists mostly in monomeric form at low concentrations, the CD spectra are always consistent (200 μM = bottom line; 300 μM = top line). (b, c and d) At 400 μM, **1** displaces various CD spectra, indicating the fibril aggregates of **1** exist in more than one morphology.

Figure 14 depicts the influence of a surfactant on self-assembly of **1**. Triton X-100 was mixed with **1** (10 mM) before and after hydrogel formation. The hydrogel of **1** can tolerate up to 0.1% Triton X-100. Treated with 0.1% Triton X-100, the fibrillar aggregates of **1** tend to cross-link with each other instead of randomly dispersing, but the width of fibrillar aggregates remains unchanged.

Figure 15 depicts the structure, cytotoxicity, and cell response of the enantiomer of **1**. In molecule **2**, L-Phe is replaced by D-Phe. Cytotoxicity of **1** and **2** are examined on HeLa cells at the concentration of 400 μM after 48 h incubation. Data are presented as mean ± SD of three independent experiments. Tubulin staining of 2 is performed on HeLa cells at the concentration of 400 μM after 24 h incubation. Scale bar = 10 μm.

Figure 16 tabulates the major components of the proteins (40 to 70 kDa on SDS-PAGE) pulled-down by hydrogel formed by **1** measured by protein mass-spectrometry. Tubulin proteins are TUBA4A and TUBB2C.

Figure 17 depicts the degradation of **1** in HeLa cells. HeLa cells were lysed after incubation with **1** at different concentrations for 12 h at 37 °C. The fragmental residue of **1** detected and quantified by LC-MS was (S)-2-(2-(naphthalen-2-yl) acetamido)-3-phenylpropanoic acid.

Figure 18 depicts the structure of compound **1**.

Figure 19 depicts an optical image of the hydrogel formed by 0.4 wt% of **1** in PBS buffer.

Figure 20 depicts fluorescence spectra of **1** in PBS buffer with increased concentration of **1** (λ_{ex} = 275 nm). a) Fluorescence spectra of **1** at 200 and 300 μM in PBS buffer with and without filtration. b) The excimer band of naphthalene group was obtained by subtraction of the fluorescence spectra of filtrated **1** from the spectra of as prepared **1** solution (λ_{ex} = 275 nm). Filtration of **1** induces little change in the emission intensity of **1** at 200 and 300 μM and there is little intensity for excimer of naphthalene at 200 and 300 μM.

Figure 21 depicts the intracellular concentration of **1** in PC12 and T98G cells after incubation with 400 μM of **1** for 12 h. Cells in exponential growth phase were seeded in a 10 cm petri dish at 10,000 cell/mL. The cells were allowed to attach for 24 h at 37 °C, 5% CO_2. The culture medium was removed, and new culture medium containing **1** at 0 or 400 μM was added. After 12 h of incubation, cells were washed with PBS buffer 3 times and collected by cell scraper with 1 mL of PBS buffer. The cell suspension was centrifuged at 600 g for 5 min to obtain a cell pellet. 10 μL of the cell pellet were lysed in 200 μL of water and 200 μL of MeOH. After centrifugation at 12,000 g for 5 min to remove insoluble proteins, the lysate suspension was collected. The concentration of **1** in the lysate was measured by LC-MS.

Figure 22 depicts the characteristics and cytotoxicity of a structural analog of **1**. Replacement of phenylalanine in **1** with tyrosine gives rise to Nap-YY (**2**) that has poorer

gelation ability and lower cytotoxicity than **1**. a) Chemical structure of **2**. b) Circular dichroism spectra of **2** at different concentrations in PBS buffer. c) TEM image of **2** at 5 mM shows the self-assembled structures of **2**. d) MTT assay of HeLa cells incubated with **2**.

Figure 23 tabulates the concentrations of **1** after filtration. [a] Following filtration, the solutions of **1** were diluted three-fold by MeOH to ensure complete dissolution of **1**. The concentration of **1** was calculated from the absorbance of the solution at 260 nm.

Figure 24 tabulates the protein composition (40 kDa to 70 kDa on SDS-PAGE) pulled-down by hydrogel formed by **1**.

DETAILED DESCRIPTION OF THE INVENTION

OVERVIEW

In certain embodiments, the invention relates to a study of the aggregates of a small hydrophobic molecule (**1**) (to distinguish these aggregates from the aggregates or oligomers of proteins, we term them as "molecular aggregates"). In certain embodiments, the molecular aggregates of **1** (Figure 6) biophysically and morphologically resemble the aggregates of aberrant protein. In certain embodiments, the molecular aggregates of **1** display extensive, non-covalent intermolecular interactions (i.e., supramolecular interactions), resulting in an exceptional capability of self-assembly to form cross-β fibrillar aggregates in aqueous medium. In certain embodiments, the invention relates to the origin of the cytotoxicity of the molecular aggregates of **1** in cancer cells in the hope to provide insights for understanding the role of protein aggregates in inverse association between cancer and Alzheimer's disease.

While the monomers of **1** are innocuous to all cell lines tested, the molecular aggregates of **1** display differential cytotoxicity towards cancer cell lines and a neuronal cell line. In other words, the aggregates sufficiently inhibit growth of the cancer cells within 48 h but have little acute toxicity on the neuronal cell line. The molecular aggregates enter the cancer cells via active transportation, accumulate in cytoplasm, and disrupt the cell cycle by arresting the cancer cells in G1/G0 phase, in addition to being able to delay cell migration. On the other hand, the neuronal cells uptake less of the molecular aggregates than the cancer cells. Protein pull-down by the hydrogel of the molecular aggregates helps discover the leads of protein targets of the aggregates of **1**. Tubulin is one of the targets. *In vitro* tubulin polymerization and cell-based assays not only confirm tubulin heterodimer as the major protein target, but also indicate that the molecular aggregates of **1** cluster short

microtubules and prevent growth of microtubules in cancer cell lines. This observation of *self-assembly* of small molecules to disrupt *self-organization* of functional proteins demonstrates an unprecedented mechanism of molecular interaction. Contrary to the case of cancer cells, **1** exhibits little observable disruption of the microtubule network of PC12. This selective cytotoxicity likely stems from not only the increased cellular uptake of cancer cells, but also the existence of neuron-rich microtubule-stabilizing proteins. Moreover, the molecular aggregates inhibit the growth of cancer cells in the xenograft tumor mice model without inducing noticeable inflammation on the mice model. The successful inhibition of xenograft tumor growth promises a new direction for developing anti-cancer drug based on the interaction between molecular aggregates and proteins. Moreover, considering the morphological and phenotypical similarity between the aggregates of **1** and the aggregates or oligomers of aberrant proteins, the molecular basis of the cytotoxicity of the aggregates of **1** implies possibility for the oligomers or aggregates of aberrant protein to exhibit acute cytotoxicity to cancer cells, as well as chronic toxicity to neural cells. The verification of this hypothesis ultimately may provide insights for understanding and treating cancer and Alzheimer disease, the two most devastating human diseases.

DISCUSSION

Cytotoxic oligomers of amyloids, although arising from different proteins and associated with different diseases, share many common properties. The similarities have driven exploration of peptide mimics of β-amyloids in the hope of providing insights regarding Alzheimer's disease and other neurodegenerative diseases. Most of the research, however, has focused on the ability of the peptide fragments (i) to form the cross-β structure, a unique morphological feature of β-amyloid, and (ii) to exhibit neurotoxicity. Although this work recreates one or two key aspects of amyloid proteins, identification of the molecular targets of the aggregates of aberrant proteins has not been possible.

Despite the fact that their building blocks are much smaller (M_r of **1** is 480 Da) than the aberrant proteins (ranging from several thousand to hundred thousand Da), the molecular aggregates of **1** share both morphological and phenotypical features with the aggregates or oligomers of the aberrant proteins. The most notable similarity is that, like the core segments of amyloids, the molecules of **1** self-assemble in water to form fibrillar aggregates that adopt cross-β structure. In addition, like amyloid oligomers, the aggregates of **1** exhibit polymorphism. As observed by CD, different batches of the solutions of **1** at

400 μM give the CD spectra with different intensity and peaks (**Fig. 13**). Although the characteristic peaks of β-sheets appear in all the CD spectra of the aggregates of **1**, indicating the β-sheet like superstructure as the core structure of molecular aggregates of **1**, the discordance of the CD measurements resembles the trait of the CD spectra of amyloid peptides, confirming that the aggregates of **1** are kinetically trapped cross-β nanofibers. Moreover, like amyloid oligomers, the aggregates of **1** also resist detergent. That is, the addition of detergent is unable to break up the aggregates of **1** (**Fig. 14**). These results suggest that the aggregates of **1** and the aggregates of aberrant proteins or the amyloid oligomers share similar thermodynamic and kinetic features.

A less noticed common feature among the aberrant protein aggregates is that they exhibit cytotoxicity at the similar weight/volume concentration. For example, the IC_{50} values of several aberrant protein aggregates (e.g., transthyretin (0.2 mg/mL), HypF-N (0.03~0.2 mg/L), and K11V-TR (0.8 mg/mL)) are mostly in the similar range (several tenths mg/mL) when they exhibit cytotoxicity. The molecular aggregates of **1** exhibit cytotoxicity at the concentrations of 400 μM, which is about 0.19 mg/mL. This coincidence also implies a common, yet unidentified origin for the cytotoxicity of the aggregates of hydrophobic molecules.

Another often overlooked feature of amyloid oligomers is that their cytotoxicity is independent of chirality of the amino acids. The enantiomer of **1** (i.e., **2**, formed by the replacement of the L-Phe with D-Phe), which has similar ability of aggregation as that of **1**, exhibits similar cytotoxicity and ability to disrupt the formation of microtubules (**Fig. 15**). These results not only exclude the possibility that the dipeptide motif acts as a specific ligand for unknown receptors to result in cell death for the case of **1**, but also indicate that the cytotoxicity of molecular aggregates of **1** is independent of chirality of the residue of the peptides. This observation suggests that molecular aggregates of **1** and amyloid oligomers share similar phenotypical features.

The morphological and phenotypical similarities between the molecular aggregates of **1** and amyloid oligomers allow the molecular aggregates of **1** to serve as a mimic of aggregates of aberrant proteins or amyloid oligomers. The molecular aggregates of **1** cluster short microtubules on their surface. The clustered short microtubules likely lack oriented arrangement. Such disorientation disfavors the connection between the short microtubules or sterically hinders the growth of microtubule fibrils. When many of tubulin heterodimers exist in clusters, the cell fails to produce sufficient amount of microtubules. The loss of

microtubules mediates cell-cycle arrestment and eventually triggers the apoptosis cascade (**Figure 7**). This result also provides a plausible detail for the interaction between tubulin and amyloid-like protein aggregates inside cells. However, multiple bands on SDS-PAGE (**Fig. 4**) imply that the interaction between molecular aggregates of 1 and cellular proteins, though have a rather specific target, is yet promiscuous. Therefore, it remains a possibility that molecular aggregates of **1** might interact with other proteins in cells to promote clustering of microtubules.

Unlike the case for cancer cells, the aggregates of **1** exhibit little acute cytotoxicity towards neuron cell line (PC12). One reason is that PC12 cells have slower metabolism and growth (e.g., doubling every 72 h) than that of cancer cells. In fact, PC12 cells accumulate much less amount of **1** than HeLa cells do (**Fig. 10b**). Another reason is that, PC12 cells, as a neuronal cell, have abundant amount of microtubule-stabilizing proteins (e.g., tau and MAP2) to promote tubulin polymerization and stabilize microtubules. Meanwhile, the pull-down assay suggests molecular aggregates of **1** has little or no interaction with tau (**Figure 16**), thus hardly disrupting the functions of tau. Therefore, the existence of microtubule-stabilizing proteins in neurons can counter the effect of the molecular aggregates of **1**, which is consistent with that PC12 cells, incubated with **1** at 400 μM (**Fig. 5p**), still display intact microtubule network. These two effects together, protect the PC12 cells from cytotoxicity induced by molecular aggregates of **1** (**Figure 7**). However, the constant supply of 400 μM of **1** causes significant loss of cell viability of PC12 cells after 7 days (**Fig. S3c**), a scenario that is similar to the chronic toxicity of amyloid oligomers in Alzheimer's disease.

The self-assembly of small molecules to disrupt self-organization of protein is a new mechanism of molecular interaction. While self-organization of tubulin heterodimers in cell is already a very complex process, characterization of the atomic-level structures of molecular aggregates of **1** is of great difficulty because of their polymorphism. Due to these two reasons, elucidating the atomistic detail of the interactions between the molecular aggregates of **1** and tubulin heterodimers remains to be a challenge. Nonetheless, selective inhibition of tumor cells over neuronal cells in cell assays and successful inhibition of tumor progression in the xenograft animal model underscore the potential of molecular aggregates of **1**, or aggregates formed by other small molecules, as a new paradigm for cancer therapy without depending on tight ligand-receptor binding. Notably, the abated cytotoxicity of **1** towards neuronal cell promises the application of **1** in targeting brain

tumors while leaving the central nerve system unharmed. Moreover, a merit of these self-assembled aggregates is that their cytotoxicity is governed by the spatiotemporal profiles of the aggregates. Unlike amyloid proteins that resist degradation and induce chronic cytotoxicity, the degradation of **1** (Fig. 17) and other small molecular aggregates are rather fast and even tunable. The spatiotemporal profiles of the molecular aggregates not only promise little chronic effect but also offer controllable cytotoxicity via tuning of aggregation.

Although it remains unable to provide a simple notion for explaining the lowered Alzheimer's disease rate in cancer patients, this study on the aggregates of **1** offers valuable insights for understanding the lowered cancer rate in Alzheimer's disease patients. The molecular aggregates of **1** induce differential and selective cytotoxicity in both cell and animal models. These results imply that amyloid oligomers, as they are similar with molecular aggregates of **1** in many aspects, might also inhibit the growth of cancer cells to result in the inverse cancer comorbidity in patients with Alzheimer's disease. Although other possible molecular mechanisms remain to be elucidated, this study offers a new perspective and a new direction for understanding the complicated inverse association between Alzheimer's disease and cancers.

DEFINITIONS

For convenience, before further description of the present invention, certain terms employed in the specification, examples and appended claims are collected here. These definitions should be read in light of the remainder of the disclosure and understood as by a person of skill in the art. Unless defined otherwise, all technical and scientific terms used herein have the same meaning as commonly understood by a person of ordinary skill in the art.

In order for the present invention to be more readily understood, certain terms and phrases are defined below and throughout the specification.

The articles "a" and "an" are used herein to refer to one or to more than one (i.e., to at least one) of the grammatical object of the article. By way of example, "an element" means one element or more than one element.

The phrase "and/or," as used herein in the specification and in the claims, should be understood to mean "either or both" of the elements so conjoined, i.e., elements that are conjunctively present in some cases and disjunctively present in other cases. Multiple elements listed with "and/or" should be construed in the same fashion, i.e., "one or more"

of the elements so conjoined. Other elements may optionally be present other than the elements specifically identified by the "and/or" clause, whether related or unrelated to those elements specifically identified. Thus, as a non-limiting example, a reference to "A and/or B", when used in conjunction with open-ended language such as "comprising" can refer, in one embodiment, to A only (optionally including elements other than B); in another embodiment, to B only (optionally including elements other than A); in yet another embodiment, to both A and B (optionally including other elements); etc.

As used herein in the specification and in the claims, "or" should be understood to have the same meaning as "and/or" as defined above. For example, when separating items in a list, "or" or "and/or" shall be interpreted as being inclusive, i.e., the inclusion of at least one, but also including more than one, of a number or list of elements, and, optionally, additional unlisted items. Only terms clearly indicated to the contrary, such as "only one of" or "exactly one of," or, when used in the claims, "consisting of," will refer to the inclusion of exactly one element of a number or list of elements. In general, the term "or" as used herein shall only be interpreted as indicating exclusive alternatives (i.e., "one or the other but not both") when preceded by terms of exclusivity, such as "either," "one of," "only one of," or "exactly one of." "Consisting essentially of," when used in the claims, shall have its ordinary meaning as used in the field of patent law.

As used herein in the specification and in the claims, the phrase "at least one," in reference to a list of one or more elements, should be understood to mean at least one element selected from any one or more of the elements in the list of elements, but not necessarily including at least one of each and every element specifically listed within the list of elements and not excluding any combinations of elements in the list of elements. This definition also allows that elements may optionally be present other than the elements specifically identified within the list of elements to which the phrase "at least one" refers, whether related or unrelated to those elements specifically identified. Thus, as a non-limiting example, "at least one of A and B" (or, equivalently, "at least one of A or B," or, equivalently "at least one of A and/or B") can refer, in one embodiment, to at least one, optionally including more than one, A, with no B present (and optionally including elements other than B); in another embodiment, to at least one, optionally including more than one, B, with no A present (and optionally including elements other than A); in yet another embodiment, to at least one, optionally including more than one, A, and at least one, optionally including more than one, B (and optionally including other elements); etc.

It should also be understood that, unless clearly indicated to the contrary, in any methods claimed herein that include more than one step or act, the order of the steps or acts of the method is not necessarily limited to the order in which the steps or acts of the method are recited.

In the claims, as well as in the specification above, all transitional phrases such as "comprising," "including," "carrying," "having," "containing," "involving," "holding," "composed of," and the like are to be understood to be open-ended, i.e., to mean including but not limited to. Only the transitional phrases "consisting of" and "consisting essentially of" shall be closed or semi-closed transitional phrases, respectively, as set forth in the United States Patent Office Manual of Patent Examining Procedures, Section 2111.03.

Certain compounds contained in compositions of the present invention may exist in particular geometric or stereoisomeric forms. In addition, polymers of the present invention may also be optically active. The present invention contemplates all such compounds, including cis- and trans-isomers, *R*- and *S*-enantiomers, diastereomers, (D)-isomers, (L)-isomers, the racemic mixtures thereof, and other mixtures thereof, as falling within the scope of the invention. Additional asymmetric carbon atoms may be present in a substituent such as an alkyl group. All such isomers, as well as mixtures thereof, are intended to be included in this invention.

If, for instance, a particular enantiomer of compound of the present invention is desired, it may be prepared by asymmetric synthesis, or by derivation with a chiral auxiliary, where the resulting diastereomeric mixture is separated and the auxiliary group cleaved to provide the pure desired enantiomers. Alternatively, where the molecule contains a basic functional group, such as amino, or an acidic functional group, such as carboxyl, diastereomeric salts are formed with an appropriate optically-active acid or base, followed by resolution of the diastereomers thus formed by fractional crystallization or chromatographic means well known in the art, and subsequent recovery of the pure enantiomers.

For purposes of this invention, the chemical elements are identified in accordance with the Periodic Table of the Elements, CAS version, Handbook of Chemistry and Physics, 67th Ed., 1986-87, inside cover.

EXEMPLARY METHODS OF THE INVENTION

In certain embodiments, the invention relates to a method of treating or preventing cancer comprising the step of

administering to a subject in need thereof a plurality of hydrophobic, self-assembling monomers.

In certain embodiments, the invention relates to any one of the aforementioned methods, wherein the cancer is a sarcoma, a carcinoma, or a lymphoma.

In certain embodiments, the invention relates to any one of the aforementioned methods, wherein the cancer is a brain tumor.

In certain embodiments, the invention relates to a method of retarding or preventing the growth of a microtubule comprising the step of

contacting tubulin with a plurality of hydrophobic, self-assembling monomers.

In certain embodiments, the invention relates to any one of the aforementioned methods, wherein the tubulin is in the form of a heterodimer. In certain embodiments, the invention relates to any one of the aforementioned methods, wherein the tubulin is in the form of an α- and β-tubulin heterodimer.

In certain embodiments, the invention relates to any one of the aforementioned methods, wherein the hydrophobic, self-assembling monomer is represented by **Formula I**:

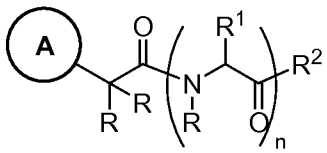

I

wherein, independently for each occurrence,

is aryl, heteroaryl, aralkyl, or heteroaralkyl;

R is H or alkyl;

R^1 is aralkyl or heteroaralkyl;

R^2 is H, alkyl, -OR, or $-NR_2$;

n is 1, 2, 3, 4, 5, 6, 7, 8, 9, 10, 11, 12, 13, 14, 15, 16, 17, 18, 19, or 20.

In certain embodiments, the invention relates to any one of the aforementioned methods, wherein 

is aryl. In certain embodiments, the invention relates to any one of

the aforementioned methods, wherein  is naphthyl. In certain embodiments, the invention relates to any one of the aforementioned methods, wherein  is 2-naphthyl.

In certain embodiments, the invention relates to any one of the aforementioned methods, wherein R is H.

In certain embodiments, the invention relates to any one of the aforementioned methods, wherein R^1 is aralkyl. In certain embodiments, the invention relates to any one of the aforementioned methods, wherein R^1 is substituted aralkyl. In certain embodiments, the invention relates to any one of the aforementioned methods, wherein R^1 is hydroxyaralkyl. In certain embodiments, the invention relates to any one of the aforementioned methods, wherein R^1 is 4-hydroxyaralkyl. In certain embodiments, the invention relates to any one of the aforementioned methods, wherein R^1 is benzyl. In certain embodiments, the invention relates to any one of the aforementioned methods, wherein R^1 is substituted benzyl. In certain embodiments, the invention relates to any one of the aforementioned methods, wherein R^1 is hydroxybenzyl. In certain embodiments, the invention relates to any one of the aforementioned methods, wherein R^1 is 4-hydroxybenzyl.

In certain embodiments, the invention relates to any one of the aforementioned methods, wherein R^2 is -OR or $-NR_2$. In certain embodiments, the invention relates to any one of the aforementioned methods, wherein R^2 is -OR. In certain embodiments, the invention relates to any one of the aforementioned methods, wherein R^2 is -OH.

In certain embodiments, the invention relates to any one of the aforementioned methods, wherein n is 1, 2, 3, 4, or 5. In certain embodiments, the invention relates to any one of the aforementioned methods, wherein n is 1, 2, or 3. In certain embodiments, the invention relates to any one of the aforementioned methods, wherein n is 2.

In certain embodiments, the invention relates to any one of the aforementioned methods, wherein the hydrophobic, self-assembling monomer is represented by:

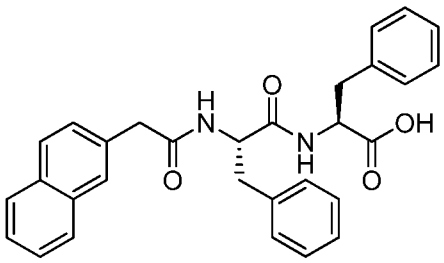

.

In certain embodiments, the invention relates to any one of the aforementioned methods, wherein the hydrophobic, self-assembling monomer is represented by:

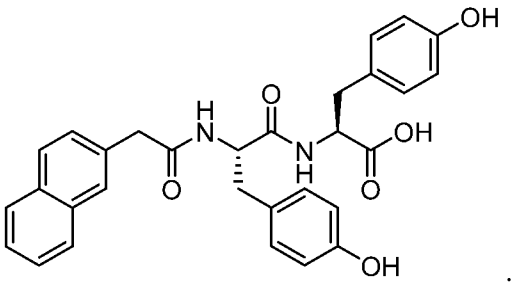

In certain embodiments, the invention relates to any one of the aforementioned methods, wherein the hydrophobic, self-assembling monomer is described in U.S. Patent Application Publication No. US 2012/0142616, PCT Patent Application Publication No. WO 2012/166705, or PCT Patent Application Publication No. WO 2012/166706, the entire contents of each of which are hereby incorporated by reference.

In certain embodiments, the invention relates to any one of the aforementioned methods, wherein the hydrophobic, self-assembling monomer comprises a dipeptide. In certain embodiments, the dipeptide comprises L-amino acids or D-amino acids.

In certain embodiments, the invention relates to any one of the aforementioned methods, wherein the hydrophobic, self-assembling monomer is present at a concentration greater than about 200 μM. In certain embodiments, the invention relates to any one of the aforementioned methods, wherein the hydrophobic, self-assembling monomer is present at a concentration greater than about 300 μM. In certain embodiments, the invention relates to any one of the aforementioned methods, wherein the hydrophobic, self-assembling monomer is present at a concentration of about 300 μM, about 320 μM, about 340 μM, about 360 μM, about 380 μM, about 400 μM, about 420 μM, about 440 μM, about 460 μM, about 480 μM, about 500 μM, about 520 μM, about 540 μM, about 560 μM, about 580 μM, or about 600 μM.

EXEMPLIFICATION

The invention now being generally described, it will be more readily understood by reference to the following examples, which are included merely for purposes of illustration of certain aspects and embodiments of the present invention, and are not intended to limit the invention.

Example 1 – General Materials and Methods

Xenograft mouse model: Nu/nu mice were injected with HeLa cells (5×10^6) subcutaneously for tumor development. Treatment was started when average tumor size

reached 30 mm^3. Mice were divided into three groups. One group (n = 3) received 0.1 mL PBS buffer as control, the other two groups (n = 4) received 0.1 mL of **1** at 5 mM or 0.5 mM. Six doses were given every three days starting day 1. Progression of tumor was monitored until 19th day of the treatment.

Hydrogel based protein pull-down assay: 4 x10^7 of HeLa cells were scrapped from petri dish and washed with PBS buffer for 3 times then centrifuged at 300 g for 5 minutes. The collected cell pellet was mixed with phosphate buffer (100 mM) then snap freeze and thaw for 3 cycles to lyse the cells. The cell lysate was clarified by centrifugation at 12,000 g for 20 min at 4 °C to remove the whole cells, nuclei and large mitochondria. 50 μL of the supernatant lysate was gently mixed with 30 μL hydrogel of **1** (10 mM in PBS buffer, pH 7.6) on rotator at RT for 30min. The hydrogel was collected by centrifugation (12,000 g, 5 min, 4 °C) and the supernatant was collected and placed on ice before analysis. The hydrogel was washed three times by gently mixing with 50 μL of the washing buffer (50 mM phosphate buffer pH 7.6 supplemented with 150 mM NaCl) on rotator at RT for 10 min followed by separation on centrifuge (12,000 g, 5 min, 4 °C). Supernatants were collected and placed on ice before analysis. Finally, the remaining hydrogel was dissolved using 1:1 washing buffer and 5X Laemeli buffer. All other samples were mixed with 5X Laemeli buffer (final concentration 2X) before SDS-PAGE.

Materials and Methods: All cell lines were obtained from ATCC. All antibodies were obtained from Abcam. Tubulin polymerization assay, tubulin and biotinylated tubulin were obtained from Cytoskeleton. Tubulin tracker and all culture media were obtained from Invitrogen. Anti-tubulin gold nanoparticles were obtained from Antibodies-Online. All other chemicals and reagents were obtained from FisherSci. Circular dichroism was performed on a JASCO J-810 spectrometer, transmission electron microscopy on Morgagni 268 transmission electron microscope, MTT viability assay and tubulin polymerization assay on DTX 880 multimode detector, flow cytometry on FACSCalibur flow cytometer, isothermal titration calorimetry on TA instrument NANO ITC Low volume, fluorescence spectra on RF-5301PC spectrofluorophotometer, confocal images on Leica SP2 microscope.

Isothermal Titration Calorimetry (ITC): 50 μL **1** in PBS buffer (pH 7.6) at 200, 300, 400 or 500 μM was diluted into 170 μL PBS buffer (pH 7.6) at a rate of 2 μL per injection and 300 s interval between each injection. The ΔH_{dil} was calculated as an average value of heat release from 20 injections.

Cell viability assay (MTT): Cells in exponential growth phase were seeded in a 96 well plate at a concentration of 50,000 cell/well. The cells were allowed to attach to the wells for 24 h at 37 °C, 5% CO_2, then the culture medium was removed and 100 μL new culture medium containing **1** at gradient concentrations was placed into each well. After culturing at 37 °C, 5% CO2 for desired time, each well was added by 10 μL of 5 mg/mL MTT ((3-(4,5-Dimethylthiazol-2-yl)-2,5-diphenyltetrazolium bromide), and the plated cells were incubate at dark for 4 h. 100 μL 10% SDS with 0.01 M HCl was added to each well to stop the reduction reaction and to dissolve the purple. After incubation of the cells at 37 °C for overnight, the viability is measured. Data represent the mean ± standard deviation of three independent experiments.

Negative staining of TEM: Carbon coated grids were glow discharged just before using to increase their hydrophilicity. The sample solution (3 μL) was place on the grid to cover the grid surface. After rinsing the grids for 10 s, a large drop of the ddH_2O was placed on parafilm and let the grid touch the water drop, with the sample-loaded surface facing the parafilm. The grid was titled, and water was gently absorbed from the edge of the grid by using a filter paper for 3 times. The grid was stained immediately by letting the grid touch a drop of 2.0 % (w/v) uranyl acetate on the parafilm with the sample-loaded surface. The grid was titled, and the stain solution was gently absorbed from the edge of the grid by using a filter paper for 3 times. The grid was allowed to dry in air for a few minutes and was examined immediately.

TEM of cell lysate: After being incubated with 500 μM of **1** for 24 h, the HeLa cells were washed with PBS buffer three times and lysed in water for 30 min. The lysate was collected and the unbroken cells were removed by centrifuge at 300 g for 5 min. $CaCl_2$ was added to the supernatant to a final concentration of 2 mM and incubate at room temperature for 30 min to disrupt microtubule that has similar diameter to molecular aggregates of **1** and thus obscure the observation. 1 μL of 1 mg/mL rabbit anti-β-tubulin@Au (in 0.01 M PBS, pH 7.4 with 10 mg/mL BSA and 0.1% sodium azide) was added to 20 μL of cell lysate, and then the solution was mixed by up and down pipetting. Negative stained TEM sample was prepared as described below.

Tubulin staining: Cells in exponential growth phase were seeded in glass bottomed culture chamber at 10,000 cell/mL. The cells were allowed for attachment for 24 h at 37 °C, 5% CO_2. The culture medium was removed, and new culture medium containing **1** at 0 or 400 μM was added. After 24 h of incubation, cells were washed with PBS buffer for 3 times

and stained by Tubulin Tracker™ Green at 100 nM and DAPI 300 nM in PBS for 30 min at 37 °C in dark. The sample was rinsed three times in PBS, and the cells were kept in PBS for imaging.

Example 2 – Characterization of the molecular aggregates

After dissolving **1** in PBS buffer (pH 7.6) in a series of dilutions, we used transmission electron microscopy (TEM) (Frado and Craig, 1992) to examine the solutions. The negatively-stained TEM image of the solution of **1** at 400 μM (**Fig. 1a**) shows fibrillar structure that have uniform width at 24±2 nm and a relatively wide distribution of the lengths with the average value of about 181 nm (**Fig. 1b**). However, the solution of **1** at 300 μM hardly shows any fibrillar structure in the TEM image (**Fig. 8**). Isothermal titration calorimetry (ITC) data agree with the results from TEM. The enthalpy of dilution of **1** (ΔH_{dil}) is a negative value as the process of dilution is exothermic. The magnitude of ΔH_{dil} of **1** becomes larger with the increase of the concentrations of **1** up to 300 μM; this trend follows the modified McMillan-Mayer model, which states that ΔH_{dil} is a monotonic function of the effective concentration of the solute (Palecz, 1998). At the concentration of 400 μM, ΔH_{dil} of **1** drastically departs from the trend and is the smallest value measured (**Fig. 1c**), indicating few monomers of **1** in the 400 μM solution of **1**. This exception agrees with that **1** exists mostly as aggregates at this concentration (i.e., 400 μM).

Circular dichroism (CD) spectrum of **1** at 400 μM shows a negative peak at 190 nm followed by a positive peak at 200 nm (**Fig. 1d**), correlating to cross-β structure according to CD simulation (Greenfield, 2006). This result coincides with the self-assembly molecular model derived from the crystal structure of **1** and, again, confirms existence of the aggregates of **1** at this concentration. At 200 μM and 300 μM, the solutions of **1** give CD signals too weak (**Fig. 1d**) to be analyzed by the CD simulation, indicating much less amount of aggregates of **1**. The CD data not only support the conclusion from TEM and ITC, but also justify the use of thioflavin T (ThT), a benzothiazole dye exhibiting enhanced fluorescence upon binding to β-sheet containing fibrils, to quantify the aggregates of **1**. As shown **Fig. 1e**, the ThT emission changes little at and below 320 μM and starts to increase in a near linear manner with the concentrations of **1** at and above 340 μM, indicating that the threshold concentration for the formation of molecular aggregates of **1** is between 320-340 μM.

Collectively, the above results confirm that a significant amount of **1** exists as the fibrillar molecular aggregates in aqueous phase when the concentration of **1** is higher than

320 μM, and the crystal structure of **1** suggests that multiple, intermolecular aromatic-aromatic interactions and intermolecular hydrogen bonding cooperatively promote **1** to self-assembly into β strand-like structures (**Figure 6**).

Example 3 - Differential cytotoxicity of the molecular aggregates

The estimation of the threshold concentration of aggregation (320-340 μM) for **1** allows us to examine the cytotoxicity of **1** in monomer and molecular aggregate forms. We first tested the cytotoxicity of **1** towards HeLa cells, the most widely studied cancer cell line, below and above the threshold concentration. While exhibiting little cytotoxicity at concentrations (200 and 300 μM) below the threshold concentration, **1**, at 400 and 500 μM, significantly decreases the viability of the HeLa cells to less than 20% within 48 h (**Fig. 2a**). The cytotoxicity of **1** towards HeLa cells significantly deviates from the sigmoidal dose response law, suggesting that the cytotoxicity of **1** at and above 400 μM unlikely stems from monomeric **1** or ligand-receptor binding that involves monomeric **1**. In addition, the removal of the molecular aggregates of **1**, by passing the medium containing **1** through a 0.22 μm PVDF filter, largely alleviates the cytotoxicity of **1** at the concentrations of 400 and 500 μM (**Fig. 2b**). These results indicate that the cytotoxicity of **1** above the threshold concentration originates from the aggregates of **1**. The extension of cell assay at 200 or 300 μM of **1** to 72 h hardly results in significant cell death (**Fig. 9a**), suggesting the monomeric **1** is cell compatible. Moreover, being incubated with other cancer cell lines (MCF-7, HepG2, T98G, U87MG, Capan-2, and MES-SA), **1** exhibits cytotoxicity in a similar manner to its effect on HeLa cell, with decreases of cell viabilities only observed at 400 and 500 μM (see **Fig. 2c, d,** and **e**; and **Fig. 9b, c,** and **d**). These results imply that the cytotoxicity of molecular aggregates of **1** and cell compatibility of monomeric **1** towards cancer cell lines is a general phenomenon. While being acutely cytotoxic to all cancer cell lines tested, **1**, at 400 and 500 μM, exhibit little toxicity towards PC12, a neuronal cell line. After being incubation with **1** at 400 and 500 μM for 7 days, PC12 cells remain largely viable (over 60%), suggesting that the molecular aggregates of **1** lack acute toxicity to PC12 (**Fig. 10a**).

To further assess the inhibitory effect of molecular aggregates of **1** to cancer cells, we inoculated HeLa cells on nude mice and treated the xenograft tumors with molecular aggregates of **1** by peritumoral injection. As shown in **Fig. 2g**, although **1** at 0.5 mM (~ 1 mg/kg) has little effect on tumor growth, **1** at 5 mM (~ 10 mg/kg) starts to inhibit tumor progression after 10th day of treatment (after 3 doses). The appearance of mice on the 19th

day of treatment evidently shows the inhibitory effect of **1** at 5 mM (**Fig. 2h** and **Fig. 11b, c** and **d**). Tumors on the mice from the group treated by 5 mM of **1** are significantly smaller than the tumor on mice from the group treated by 0.5 mM of **1** and the control group. Moreover, the surface of the skin covering and around the tumor is intact (with no ulceration or sclerosis) on every mice treated with 5 mM of **1**, and their body weights are similar with mice in control group (**Fig. 11a**), indicating that the molecular aggregates unlikely elicit inflammation response in skin tissue of the mice or cause any severe side effects.

Example 4 - Cellular response of cancer cells towards the molecular aggregates

The cytotoxicity of the molecular aggregates of **1** toward the cancer cells in cell assays and on animal model warrants further examination on the mechanism of the cell death. Since both extracellular stimuli and intracellular signaling regulate cell-cycle and cell migration, we examined whether the aggregates of **1** enter the HeLa cells. We measured the intracellular concentrations of **1** in the lysate of the HeLa cells incubated with 300 μM and 400 μM of **1** for 24 h (**Fig. 3a**) at 37 °C or 4 °C. Based on the amount of **1**, measured by liquid chromatography-mass spectroscopy (LC-MS) and the estimated total cell volume, the concentration of **1** inside the cells is about 150% of the concentration of **1** used for the incubation at 37 °C. But, at 4 °C, there is much less of **1** (about 30% of the incubating concentration) inside the cells than outside the cells (in the culture media). This result implies the accumulation of both monomers and the aggregates of **1** inside cells likely via processes of active transport.

To determine the process of cell death induced by the aggregates of **1**, we used FITC conjugated annexin V and propidium iodide (PI) to stain the cells (**Fig. 3b**). Being membrane impermeable, PI discriminates viable cells from late apoptotic or necrotic cells, and FITC conjugated annexin V binds to plasma membrane of apoptotic and necrotic cells as the former ones have extracellular exposed phosphatidylserine and the latter ones lose membrane integrity. Unlike induced necrotic cells that can be stained by both dyes and viable cells that exclude both dyes, most of the HeLa cells treated by 400 μM of **1** for 36 h exclude PI, but their plasma membranes are stained green by FITC annexin V, indicating that the aggregates of **1** induce apoptosis of the HeLa cells.

Because apoptosis associates with cell cycle, we examined the effect of the aggregates of **1** on the cell cycle. **Fig. 3d** shows the flow cytometry cellcycle analysis of the HeLa cells incubated with **1** at different concentrations. The cell-cycle distribution of the

HeLa cells incubated with 300 μM of **1**, showing a large peak of G0/G1 phase and a small peak of G2/M phase that are connected by the S phase, is similar to the cell-cycle distribution of the untreated HeLa cells. The cell-cycle distribution of the HeLa cells incubated with 400 μM of **1** indicates significant decrease of the peaks of S phase and G2/M phase. Thus, the aggregates of **1** arrest the HeLa cells at the G1/G0 phase and consequently prevent cell mitosis. The slight right shift of the whole spectra results from the overlapping of emission of 7-AAD and **1** (**Fig. 3c**). But such shift barely hampers the distribution of cell-cycle of the spectra. The aggregates of **1** also delay the migration of the HeLa cells. As shown in cell migration assay (**Fig. 3e**), after 18 h of culture, the untreated cells and the cells incubated with 300 μM of **1** exhibit similar migration rates and cover 47% of the gaps. After incubation with 400 or 500 μM of **1** for 18 h, the HeLa cells only cover 27% of the gaps, indicating that the aggregates of **1** delay the migration of the cells.

Example 5 - Protein targets of the molecular aggregates

That **1** enters the cells to affect cell cycle, cell migration, and eventually cell viability implies the interactions between the aggregates of **1** and certain intracellular proteins. Thus, we modified a hydrogel based protein pull-down assay tailored for evaluating the interactions of the aggregates of **1** with intracellular proteins (**Fig. 4**). As shown in **Fig. 4**, hydrogel based protein pull-down assay consists of the following major steps: (1) incubating the hydrogel with a cell lysate; (2) separating the hydrogel; (3) removing the non-specific proteins; (4) analyzing the proteins (by SDS-PAGE, gel staining, and Western blot). The hydrogel of **1** consists of long and entangled fibrils, formed by the self-assembly of **1**, that have diameter of 24 nm and cross-β structure, thus the hydrogel of **1** acts as an equivalent of the high density aggregates of **1**. Also, it is easy to separate the hydrogel particles from aqueous solution by centrifuging after they interact with the proteins.

The hydrogel-based protein pull-down assay (**Fig. 4**) suggests that the aggregates of **1** interact with tubulins. Silver stain reveals that three major protein bands (within the molecular weight range of 37~75 kDa) arise from the proteins in sample B, but not from the proteins in sample W3, indicating that these three bands correspond to the proteins bound specifically to the aggregates of **1**. Coomassie stain of the three bands within 37~75 kDa indicates that the intensities of the bands decrease in the order of the top band (55 kDa), the bottom band (42 kDa), and the middle band (50 kDa). Because the molecular weights of tubulin and actin are around 55 kDa and 42 kDa, respectively, and our previous result

indicates that a hydrogel formed by a small molecule, which is structurally similar with **1**, binds with tubulin, and that these two proteins are tightly related to cell cycle and cell migration, we used anti-α-tubulin and anti-actin for Western blot. Western blot proves the existence of tubulin and actin in sample B, thus confirming the selective interaction between tubulin and actin with the aggregates of **1**. In addition, the absence of tubulin in all wash-off solutions indicates that tubulin has higher affinity to the aggregates of **1** than actin does. Sample B retains only a small amount of actin, suggesting low binding affinity of actin to the aggregates of **1**. At lower molecular weight range, several bands come from both the sample B and the sample W3, indicating that these proteins bind to the aggregates of **1** with low affinity and easily dissociate into aqueous medium. In the GAPDH control, the absence of GAPDH in W2, W3, and B (**Fig. 4**) validates that the washing steps successfully remove non-specific bound proteins from the hydrogel of **1**.

As the major function of tubulin is to polymerize into microtubule, we carried out in vitro tubulin polymerization assay to evaluate how the molecular aggregates of **1** affect the polymerization of tubulin. We incubated tubulin heterodimers (i.e., the α- and β-tubulin heterodimer, existing almost exclusively in heterodimer form in cytoplasm) with **1** at different concentrations and monitored the formation of microtubule (**Fig. 5**). As shown in **Fig. 5a**, at 200 μM of **1**, the polymerization curve of tubulin almost overlaps with that of control (i.e., normal polymerization with polymerization cocktail only). At 300 μM of **1,** the polymerization curve starts to deviate slightly from the control curve. At 400 and 500 μM of **1** (i.e., molecular aggregates of **1** dominate), the polymerization curves significantly deviate from the control curve. According to the rate of exponential growth phase (V_{max}) (**Fig. 5b**), while 200 μM or 300 μM of **1** barely inhibits the polymerization of tubulins, 400 or 500 μM of **1** drastically decreases the V_{max} of the polymerization of tubulins. According to the final amount of polymers (i.e., microtubule), while 300 μM of **1** slightly decreases the amount of microtubules, 400 or 500 μM of **1** also significantly reduces the formation of microtubules (about 30% decrease) (**Fig. 5b**). To confirm that the molecular aggregates of **1**, but not monomeric **1**, inhibit the formation of microtubules, we filtrated of the reaction mixture by a 0.22 μm PVDF filter before the addition of tubulins. As shown in **Fig. 5c**, filtration of the reaction cocktail (control) hardly exhibits any effect on the polymerization of tubulins, indicating that the filtration barely disturbs tubulin polymerization. However, filtrated reaction mixtures containing 200 to 500 μM of **1** has similar polymerization curve to that of control. According to the calculated V_{max} and the final amount of polymers of

tubulins (**Fig. 5d**), 400 or 500 μM of **1**, after the filtration, only causes slight decreases in both V_{max} and the final amount of polymers of tubulins. Because filtration significantly minimized the inhibitory effect of 400 or 500 μM of **1** to tubulin polymerization, the molecular aggregates of **1** inhibit the formation of microtubules.

Microtubules are highly dynamic, growing and shrinking at a constant rate. To determine whether molecular aggregates of **1** achieve the inhibition of microtubule formation through preventing microtubule growth or accelerating microtubule shrinkage, we applied **1** to the polymerization mixture after most of tubulin heterodimers already formed microtubules (60 min of pre-incubation) and monitored the change of microtubules. As shown in **Fig. 5e**, the addition of buffer alone (control) induces little change to the microtubule, indicating that the dilution of reaction mixture barely causes any loss of microtubules. The addition of **1** (final concentration 200 to 500 μM) also induces little notable loss of microtubules. This result, being similar to that of the control, indicates that the molecular aggregates of **1** inhibit microtubule formation by preventing the growth rather than by promoting the shrinkage of microtubules.

TEM images of the aggregates of **1** incubated with tubulin heterodimers confirm the interactions between the two. The TEM images of 400 μM of **1** incubated with tubulin heterodimer (20 μM, similar to the intracellular concentration of tubulin) at 25 °C show that round dots, attaching not only on the surface but also at the ends the aggregates of **1**, connects the fibrillar aggregates of **1** into network (**Fig. 5f**). The dots have a diameter about 13±2 nm, which is larger than the size of tubulin heterodimer (8 nm in length), suggesting the presence of multiple tubulins heterodimers. The molecular aggregates of **1** have a narrower width than those formed in PBS buffer (**Fig. 1a**) because the incubations were carried in general tubulin buffer, which differs from that PBS buffer both in composition and pH. To confirm the dots on the aggregates of **1** are tubulin, we repeated the incubation with biotinylated tubulin heterodimers and then added streptavidin conjugated gold nanoparticles to the solution. As shown in the TEM images, the gold nanoparticles appear almost exclusively on or near the aggregates of **1** (**Fig. 12a**). In the absence of biotinylated tubulin heterodimers, no gold nanoparticle attaches to the aggregates of **1** (**Fig. 12b**). These results prove the presence of tubulin heterodimers on the aggregates of **1**. In another experiment, we used anti-tubulin-gold nanoparticles to label tubulin in lysate of HeLa cells treated with 500 μM of **1** for 24 h. TEM image reveals that fibril-like structures, which evidently differ from those of microtubules, attached with gold nanoparticles (**Fig. 12c**),

suggesting that the interactions between molecular aggregates of **1** and tubulin heterodimers might also occur inside cells.

Example 6 - The molecular aggregates interact with cytoskeletal proteins in cells

To confirm that the aggregates of **1** clusters multiple tubulin heterodimers and inhibit the formation of microtubules inside live cells, we used a tubulin tracker that selectively binds to tubulin polymers (microtubules) over tubulin monomers to stain the HeLa cells treated with **1** at different concentrations for 24 h. The time dependent viability of the HeLa cells treated with **1** at 400 and 500 μM indicates little loss of cell viability until after 38 h of incubation (**Fig. 5g**). Thus, at 24 h of incubation, the change in the morphology of microtubule (unlikely resulted from cell death) reveals the interaction between the molecular aggregates of **1** and tubulins. As shown in **Fig. 5h**, the untreated cells (i.e., the control) displays long, smooth microtubule fibrils stretching through the cell body. The microtubules in the HeLa cells treated with 200 μM of **1** (**Fig. 5i**) exhibit essentially the same morphology and distribution as those in the control cells. In the HeLa cells treated with 300 μM of **1**, the microtubules extend cross the cell body, but a small amount of the microtubules appear to be shorter than those in the control cells (**Fig. 5j**). This result coincides with the observation that **1**, at 300 μM, slightly decreases the final amount of the microtubules in the *in vitro* tubulin polymerization assay (**Fig. 5b**). As shown in **Fig. 5k**, the dominate morphology of tubulins, in the HeLa cells treated with 400 μM of **1**, is large clusters surrounded by scattered microtubule fibrils, which differs completely from that of the control. As the tubulin tracker only stains microtubule (i.e., polymerized tubulin heterodimers), the fluorescence from the cluster indicates the tubulin heterodimers in the clusters are short microtubules. Upon incubation with medium that initially contains 400 μM of **1** but filtered by 0.22 μm PVDF membrane, the cells display (almost) normal microtubule networks, with only few clusters (**Fig. 5l**). These observations, together with the results from tubulin polymerization assay and TEM images, demonstrate that the molecular aggregates of **1** cluster tubulin heterodimers in the form of short microtubules and prevent the growth of microtubules (**Figure 6**). The loss of microtubules induced by molecular aggregates of **1** explains the origins of the delay of cell migration and the arrest of cell-cycle in HeLa cells incubated with 400 or 500 μM of **1**. In addition, upon incubation with 400 μM of **1**, T98G cells, a glioblastoma cell line, also have disrupted microtubule network and show clusters of short microtubules (**Fig. 5n**). Unlike in HeLa and T98G cells, the microtubules in the PC12 cells treated by 400 μM of **1** still form intact microtubule

networks (**Fig. 5p**) that span through the cell body and exhibit little difference with that in the untreated PC12 cells (**Fig. 5o**), suggesting there is insignificant disruption of the formation of microtubules by the aggregates of **1** in PC12 cells after 24 h incubation with **1** at 400 μM.

INCORPORATION BY REFERENCE

All of the U.S. patents and U.S. patent application publications cited herein are hereby incorporated by reference.

EQUIVALENTS

Those skilled in the art will recognize, or be able to ascertain using no more than routine experimentation, many equivalents to the specific embodiments of the invention described herein. Such equivalents are intended to be encompassed by the following claims.

We claim:

1. A method of treating or preventing cancer, comprising the step of:

administering to a subject in need thereof a plurality of hydrophobic, self-assembling monomers.

2. The method of claim 1, wherein the cancer is a sarcoma, a carcinoma, or a lymphoma.

3. The method of claim 1, wherein the cancer is a brain tumor.

4. A method of retarding or preventing the growth of a microtubule, comprising the step of:

contacting tubulin with a plurality of hydrophobic, self-assembling monomers.

5. The method of claim 4, wherein the tubulin is in the form of a heterodimer.

6. The method of claim 4, wherein the tubulin is in the form of an α- and β-tubulin heterodimer.

7. The method of any one of claims 1-6, wherein the hydrophobic, self-assembling monomer comprises a dipeptide.

8. The method of any one of claims 1-6, wherein the hydrophobic, self-assembling monomer is represented by **Formula I**:

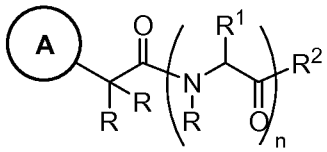

I

wherein, independently for each occurrence,

 is aryl, heteroaryl, aralkyl, or heteroaralkyl;

R is H or alkyl;

R^1 is aralkyl or heteroaralkyl;

R^2 is H, alkyl, -OR, or $-NR_2$;

n is 1, 2, 3, 4, 5, 6, 7, 8, 9, 10, 11, 12, 13, 14, 15, 16, 17, 18, 19, or 20.

9. The method of claim 8, wherein  is aryl.

10. The method of claim 8, wherein  is naphthyl.

11. The method of claim 8, wherein  is 2-naphthyl.

12. The method of any one of claims 8-11, wherein R is H.

13. The method of any one of claims 8-12, wherein R^1 is aralkyl.

14. The method of any one of claims 8-12, wherein R^1 is substituted aralkyl.

15. The method of any one of claims 8-12, wherein R^1 is hydroxyaralkyl.

16. The method of any one of claims 8-12, wherein R^1 is benzyl.

17. The method of any one of claims 8-12, wherein R^1 is substituted benzyl.

18. The method of any one of claims 8-12, wherein R^1 is hydroxybenzyl.

19. The method of any one of claims 8-12, wherein R^1 is 4-hydroxybenzyl.

20. The method of any one of claims 8-19, wherein R^2 is -OR or $-NR_2$.

21. The method of any one of claims 8-19, wherein R^2 is -OR.

22. The method of any one of claims 8-19, wherein R^2 is -OH.

23. The method of any one of claims 8-22, wherein n is 1, 2, 3, 4, or 5.

24. The method of any one of claims 8-22, wherein n is 1, 2, or 3.

25. The method of any one of claims 8-22, wherein n is 2.

26. The method of any one of claims 1-6, wherein the hydrophobic, self-assembling monomer is represented by:

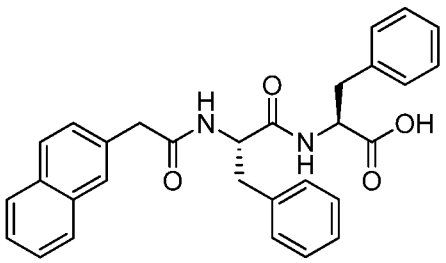

27. The method of any one of claims 1-6, wherein the hydrophobic, self-assembling monomer is represented by:

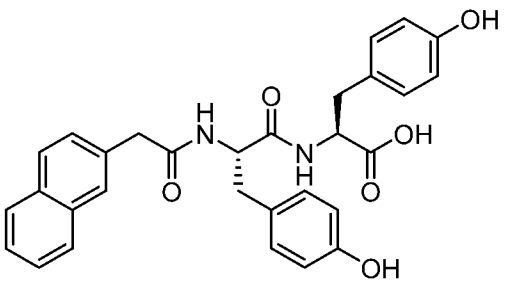

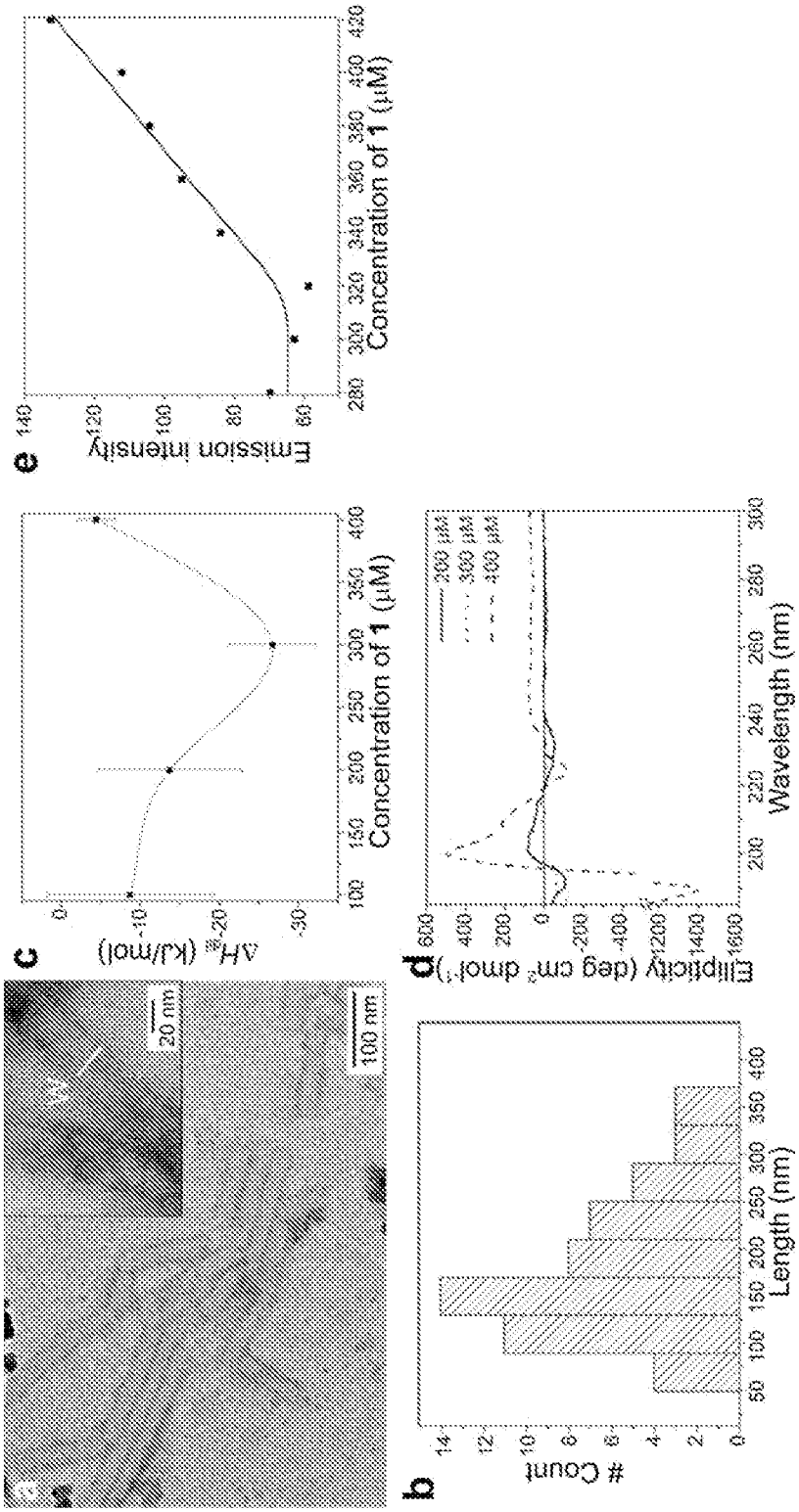
a
20 nm
100 nm
b
Count
Length (nm)
c
ΔH_ITC (kJ/mol)
Concentration of 1 (μM)
d
Ellipticity (deg cm² dmol⁻¹)
Wavelength (nm)
300 μM
300 μM
400 μM
e
Emission intensity
Concentration of 1 (μM)

Figure 1

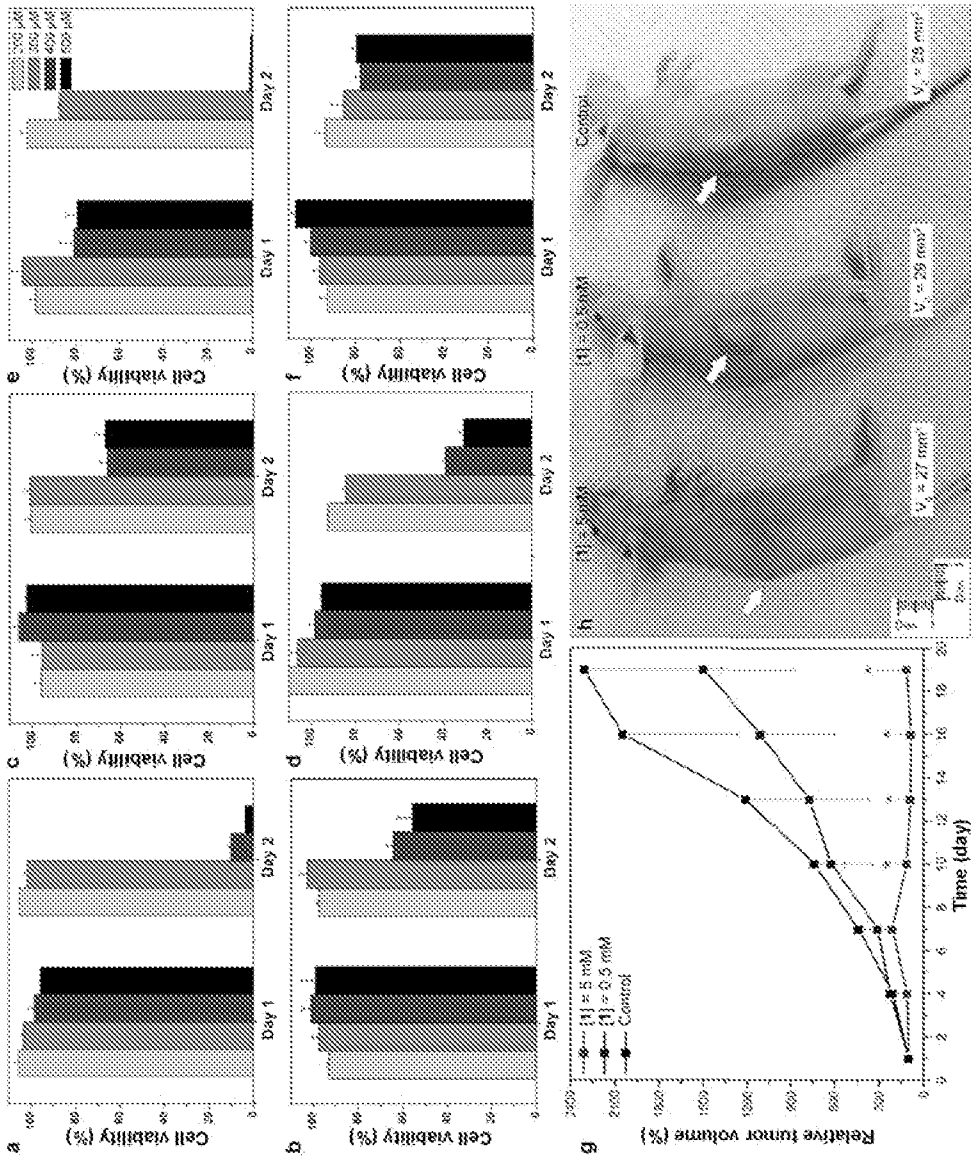
a
b
c
d
e
f
g
h
Cell viability (%)
Day 1
Day 2
Relative tumor volume (%)
Time (day)
[1] = 5 mM
[1] = 2.5 mM
Control
Control
[1] = 5 mM
[1] = 2.5 mM
V0 = 27 mm³
V0 = 29 mm³
V0 = 29 mm³

Figure 2

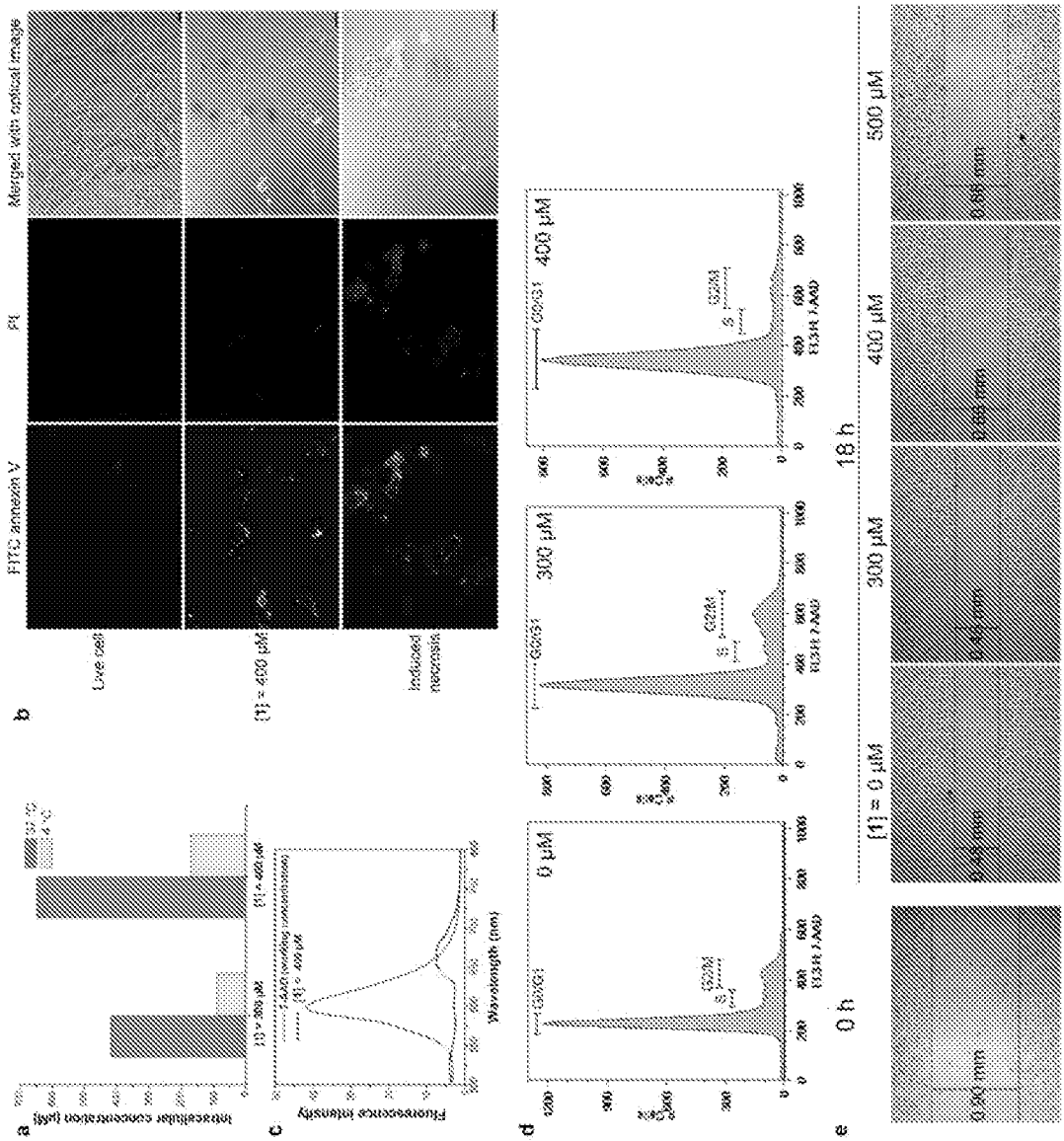
a
b
c
d
e
FITC annexin V
PI
Merged with optical image
Live cell
[1] = 400 µM
Induced necrosis
Intracellular concentration (µM)
Fluorescence intensity
Wavelength (nm)
0 µM
300 µM
400 µM
500 µM
0 h
18 h
0.50 mm

Figure 3

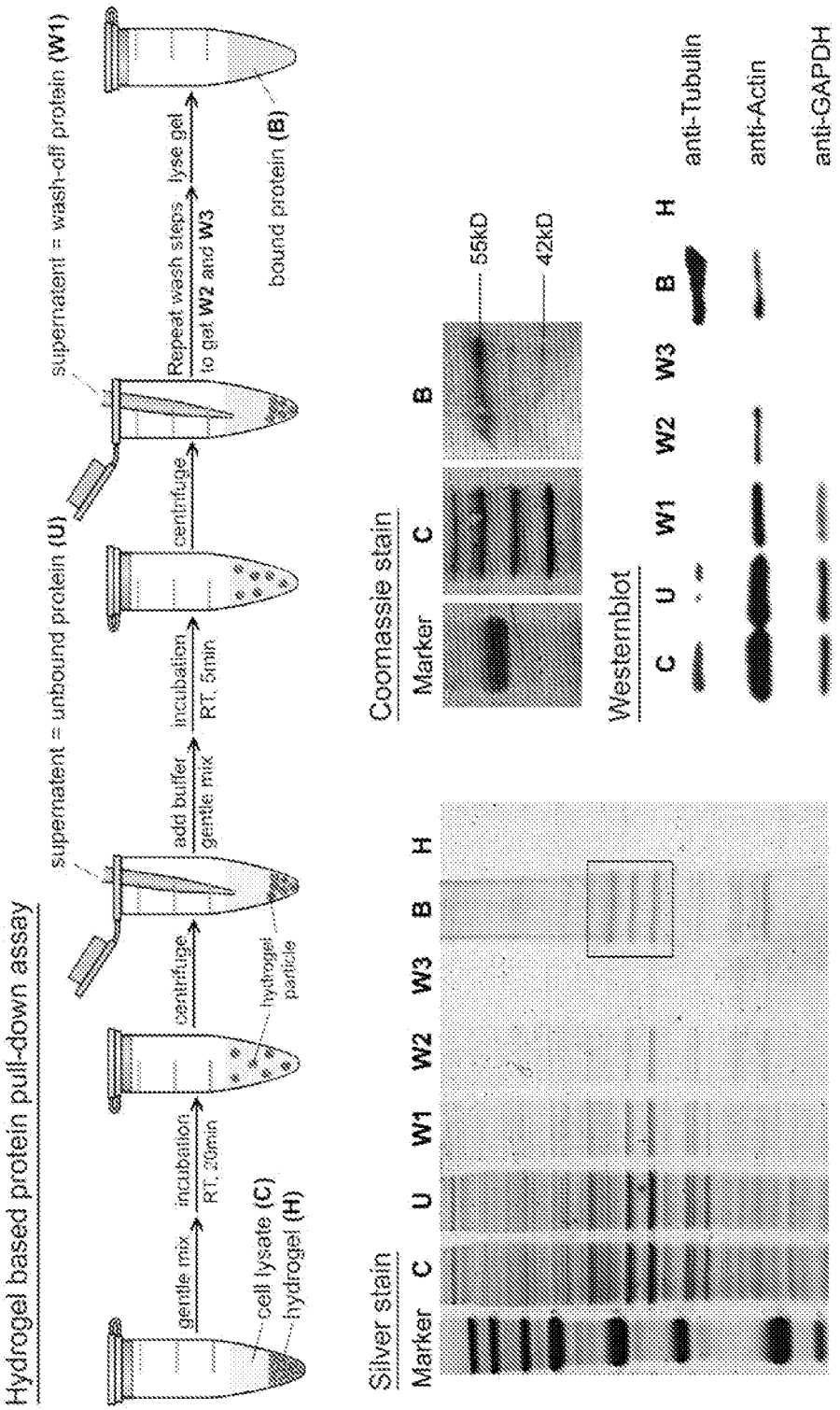
Hydrogel based protein pull-down assay
cell lysate (C)
hydrogel (H)
gentle mix
incubation
RT, 20min
centrifuge
hydrogel particle
supernatant = unbound protein (U)
add buffer
gentle mix
incubation
RT, 5min
centrifuge
supernatant = wash-off protein (W1)
Repeat wash steps
to get W2 and W3
lyse gel
bound protein (B)
Silver stain
Marker C U W1 W2 W3 B H
Coomassie stain
Marker C B
55kD
42kD
Westernblot
C U W1 W2 W3 B H
anti-Tubulin
anti-Actin
anti-GAPDH

Figure 4

Figure 5

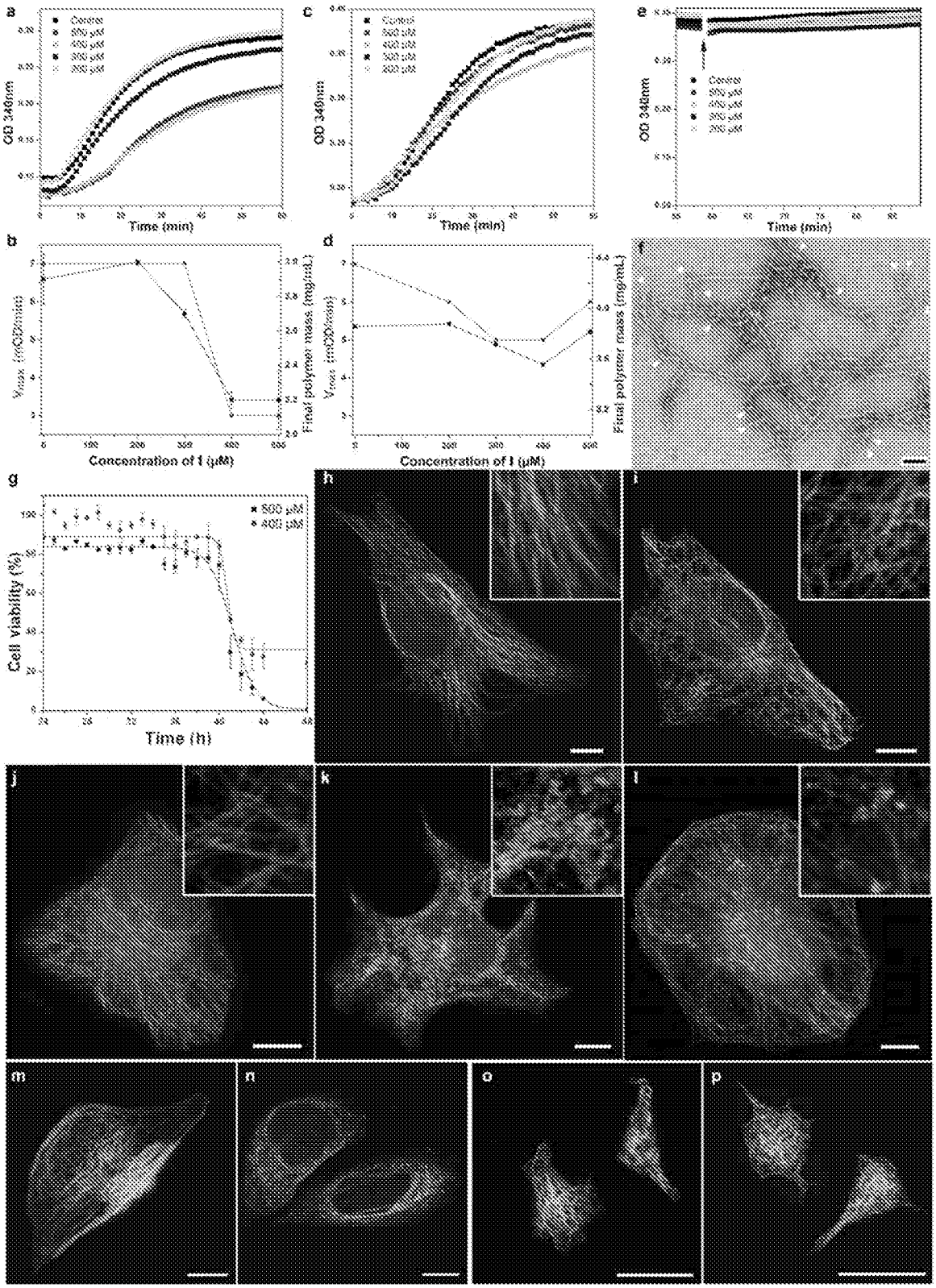
a
Control
800 μM
600 μM
400 μM
200 μM
OD 340nm
Time (min)
c
Control
800 μM
600 μM
400 μM
200 μM
OD 340nm
Time (min)
e
Control
800 μM
600 μM
400 μM
200 μM
OD 340nm
Time (min)
b
Vmax (mOD/min)
Final polymer mass (mg/mL)
Concentration of I (μM)
d
Vmax (mOD/min)
Final polymer mass (mg/mL)
Concentration of I (μM)
f
g
800 μM
400 μM
Cell viability (%)
Time (h)
h
i
j
k
l
m
n
o
p

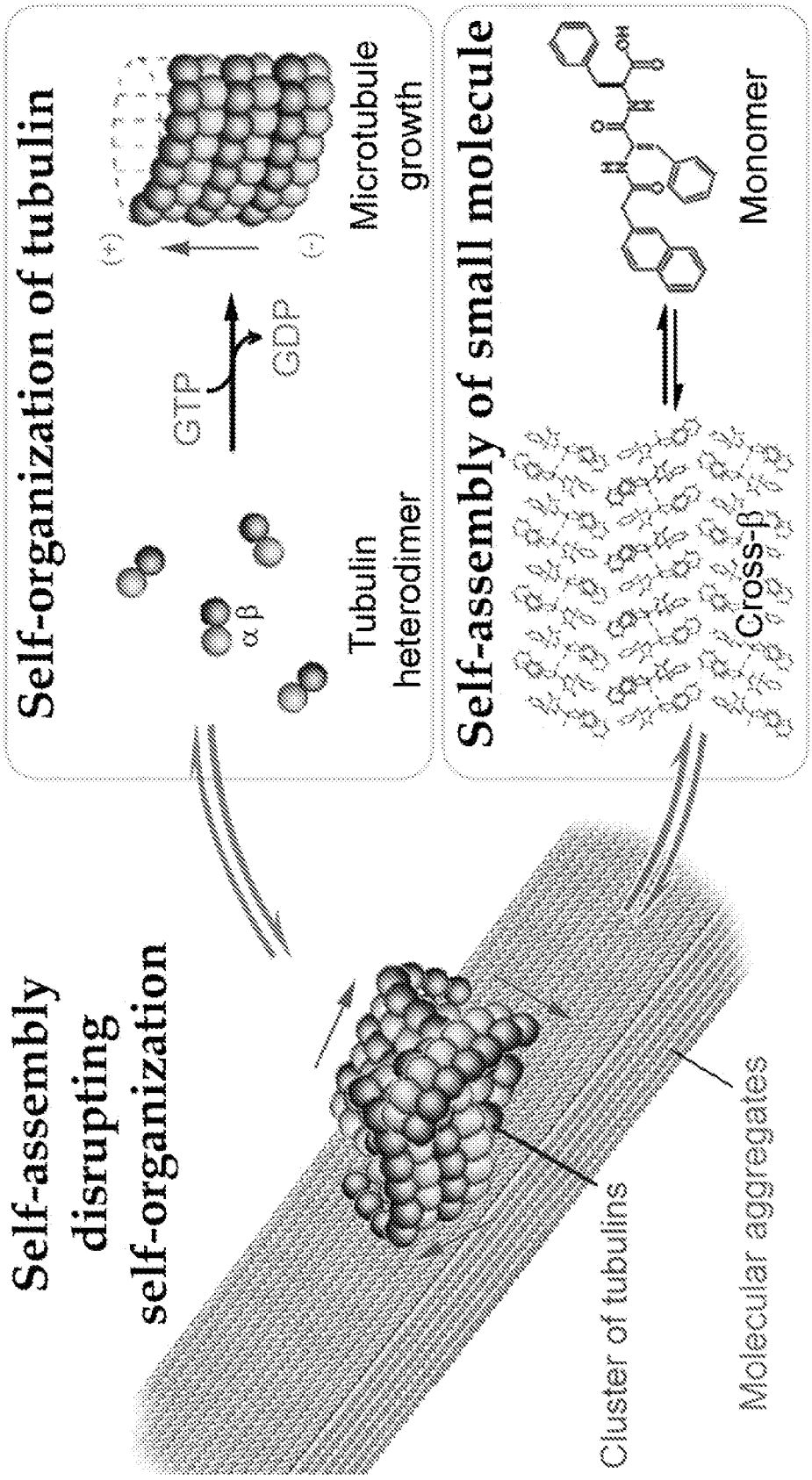
Self-organization of tubulin
GTP
GDP
Microtubule growth
Tubulin heterodimer
α β
Self-assembly of small molecule
Monomer
Cross-β
Self-assembly disrupting self-organization
Cluster of tubulins
Molecular aggregates

Figure 6

Figure 7

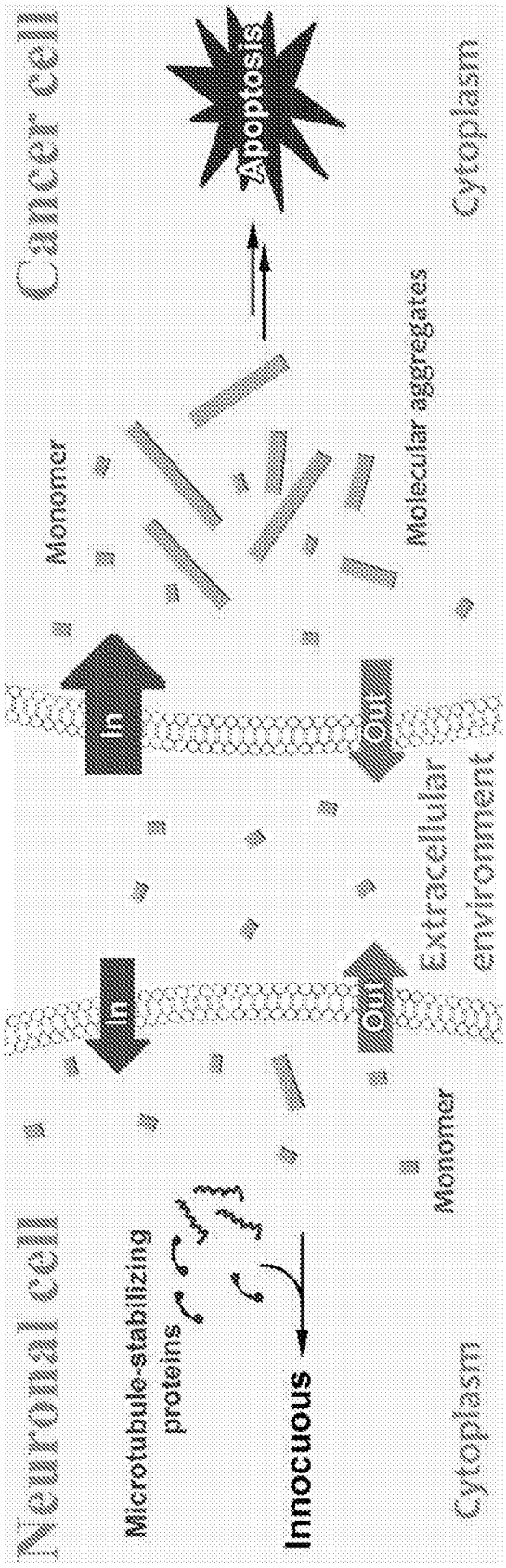
Neuronal cell
Cancer cell
Microtubule-stabilizing proteins
Innocuous
In
Out
Monomer
Molecular aggregates
Apoptosis
Extracellular environment
Cytoplasm
Cytoplasm

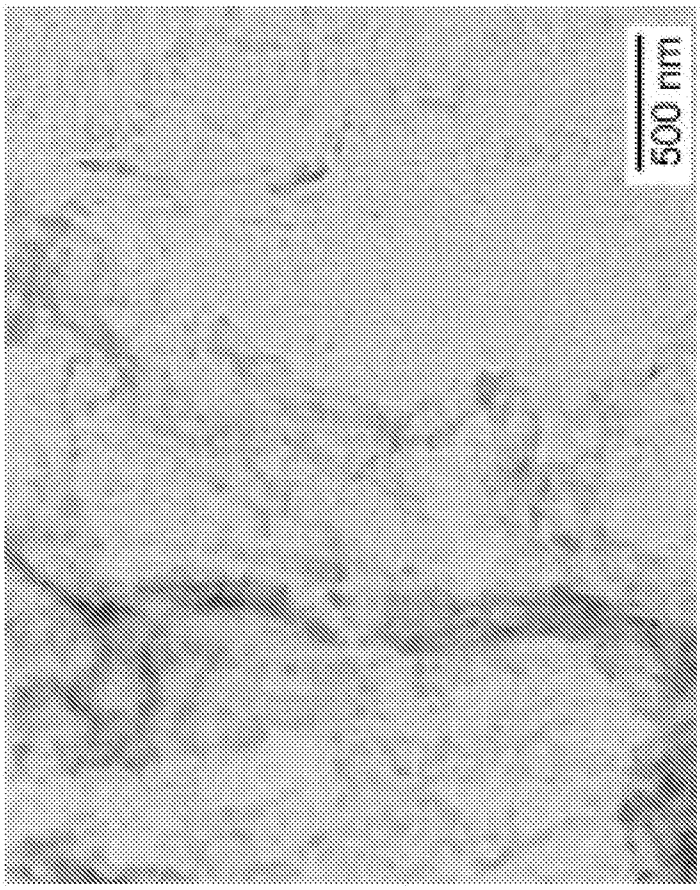

Figure 8

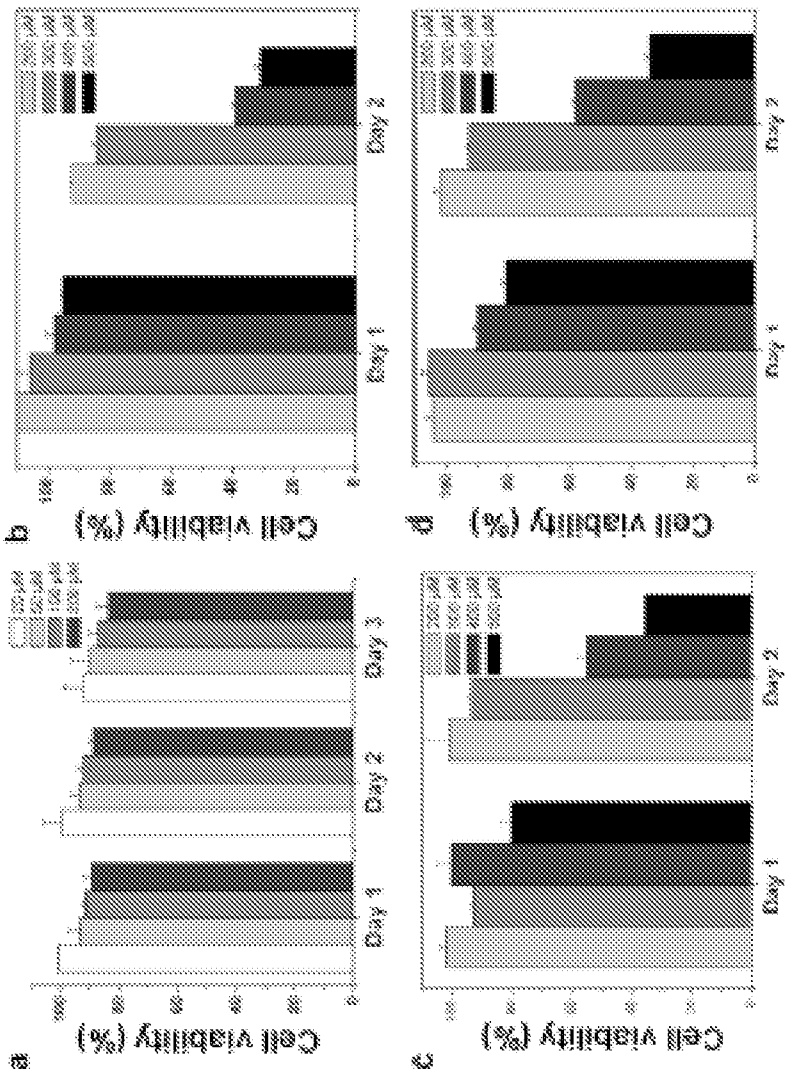
a
Cell viability (%)
Day 1
Day 2
Day 3
b
Cell viability (%)
Day 1
Day 2
c
Cell viability (%)
Day 1
Day 2
d
Cell viability (%)
Day 1
Day 2

Figure 9

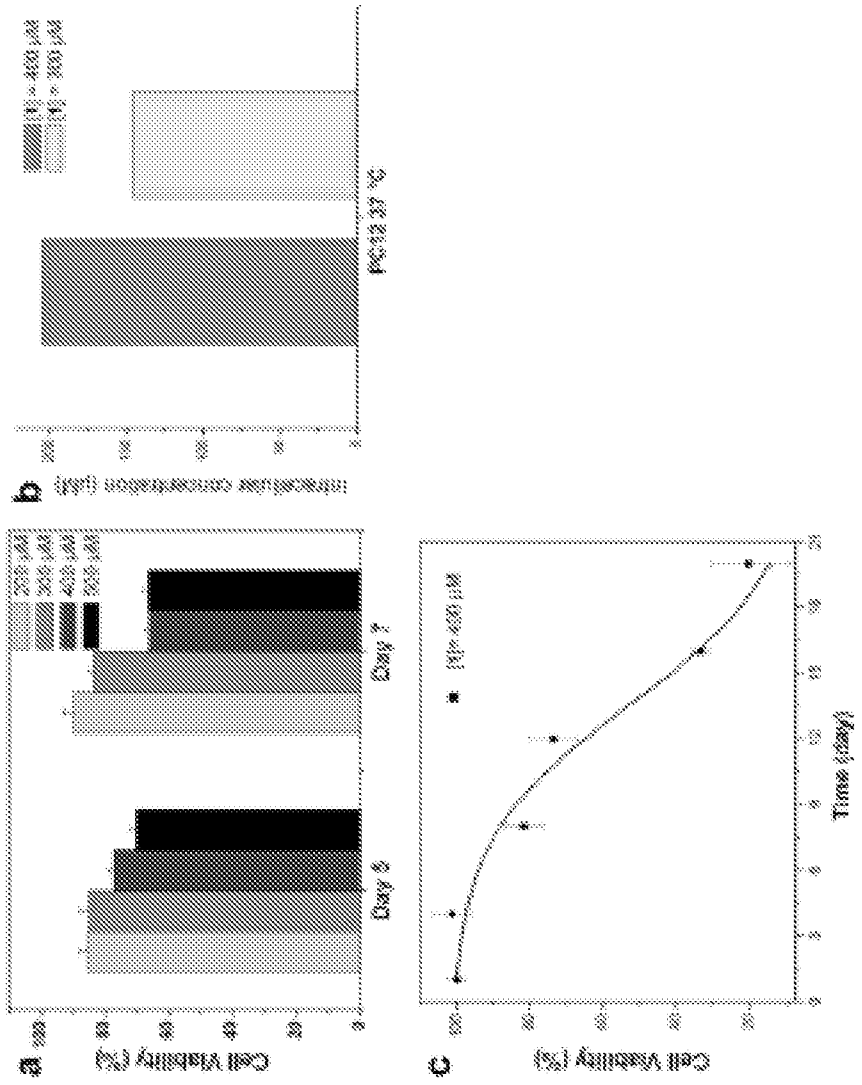
a
Cell Viability (%)
Day 2
Day 7
b
Intracellular concentration (μM)
PC-12 37 °C
c
Cell Viability (%)
Time (day)

Figure 10

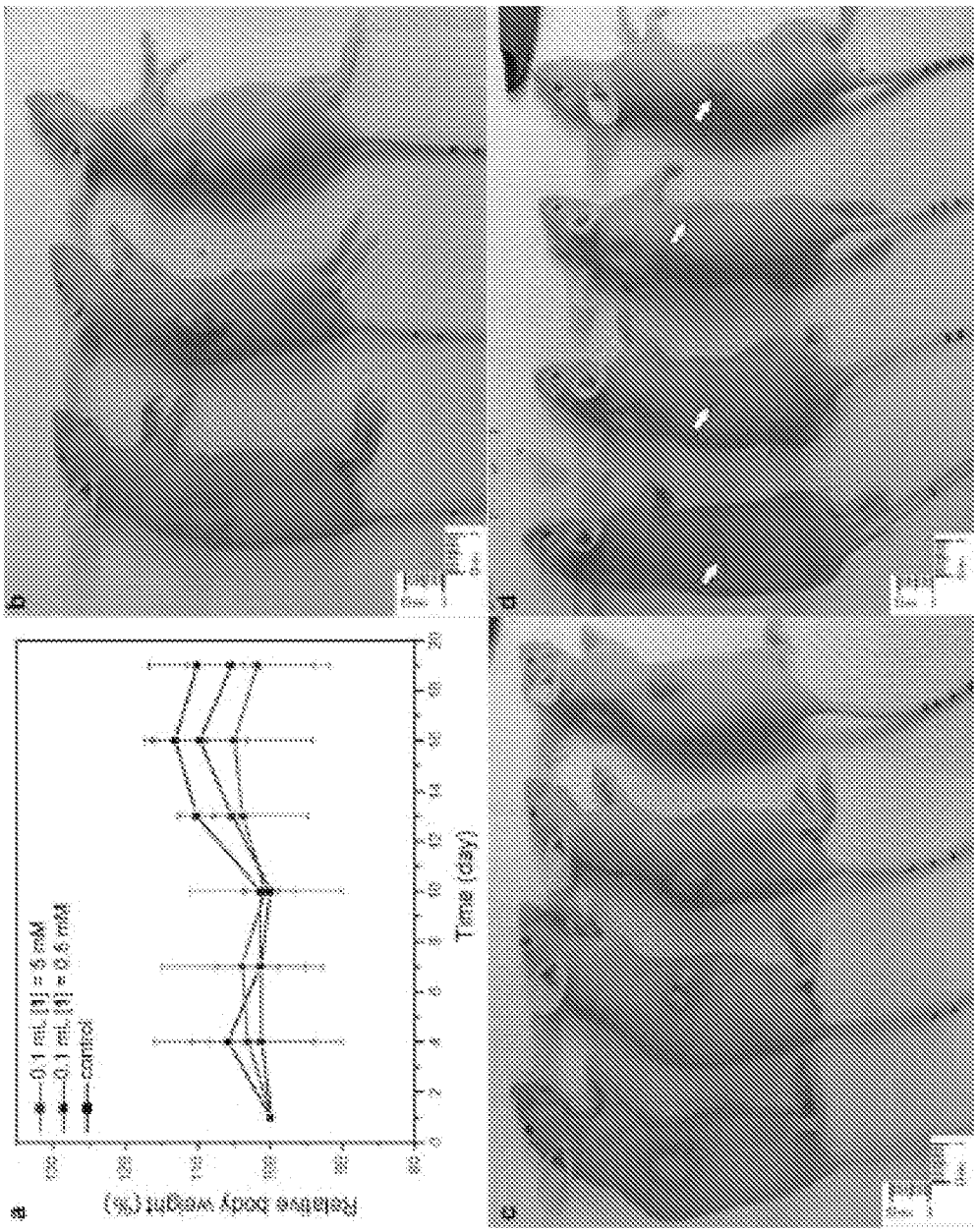
a
Relative body weight (%)
Time (day)
0.1 mL [1] = 5 mM
0.1 mL [1] = 0.5 mM
control
b
c
d

Figure 11

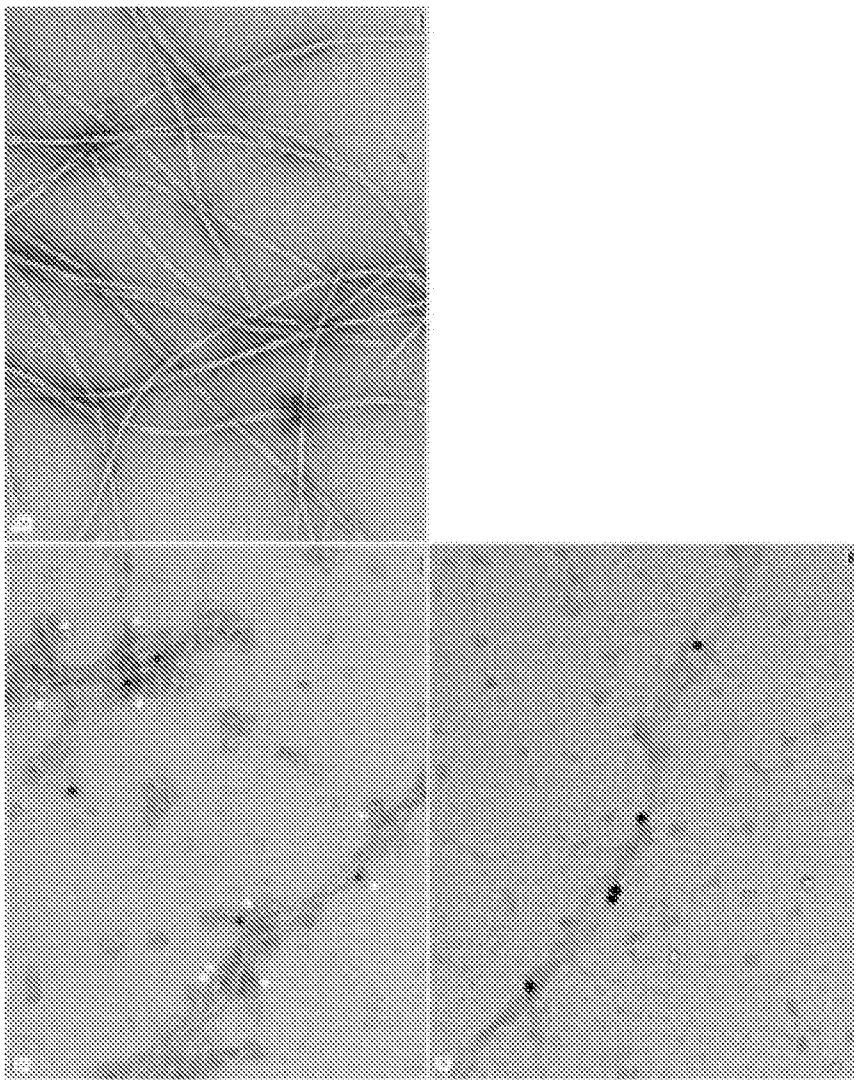

Figure 12

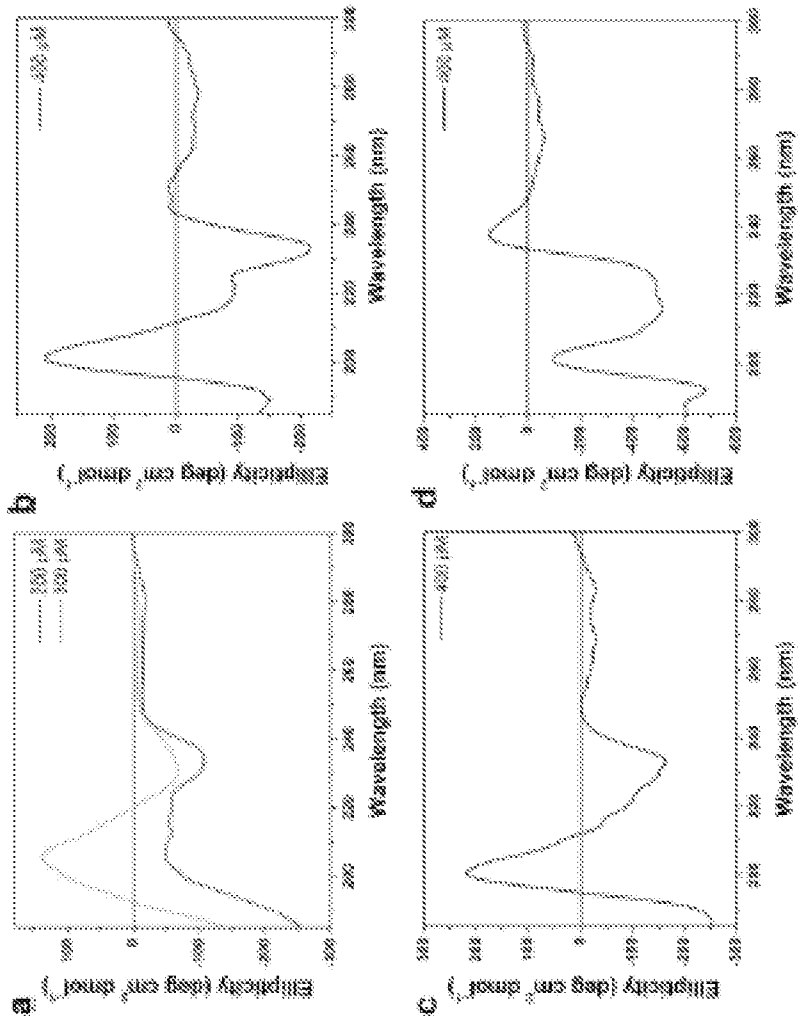
a
b
c
d
Ellipticity (deg cm² dmol⁻¹)
Wavelength (nm)
350 nM
320 nM
300 nM
400 nM

Figure 13

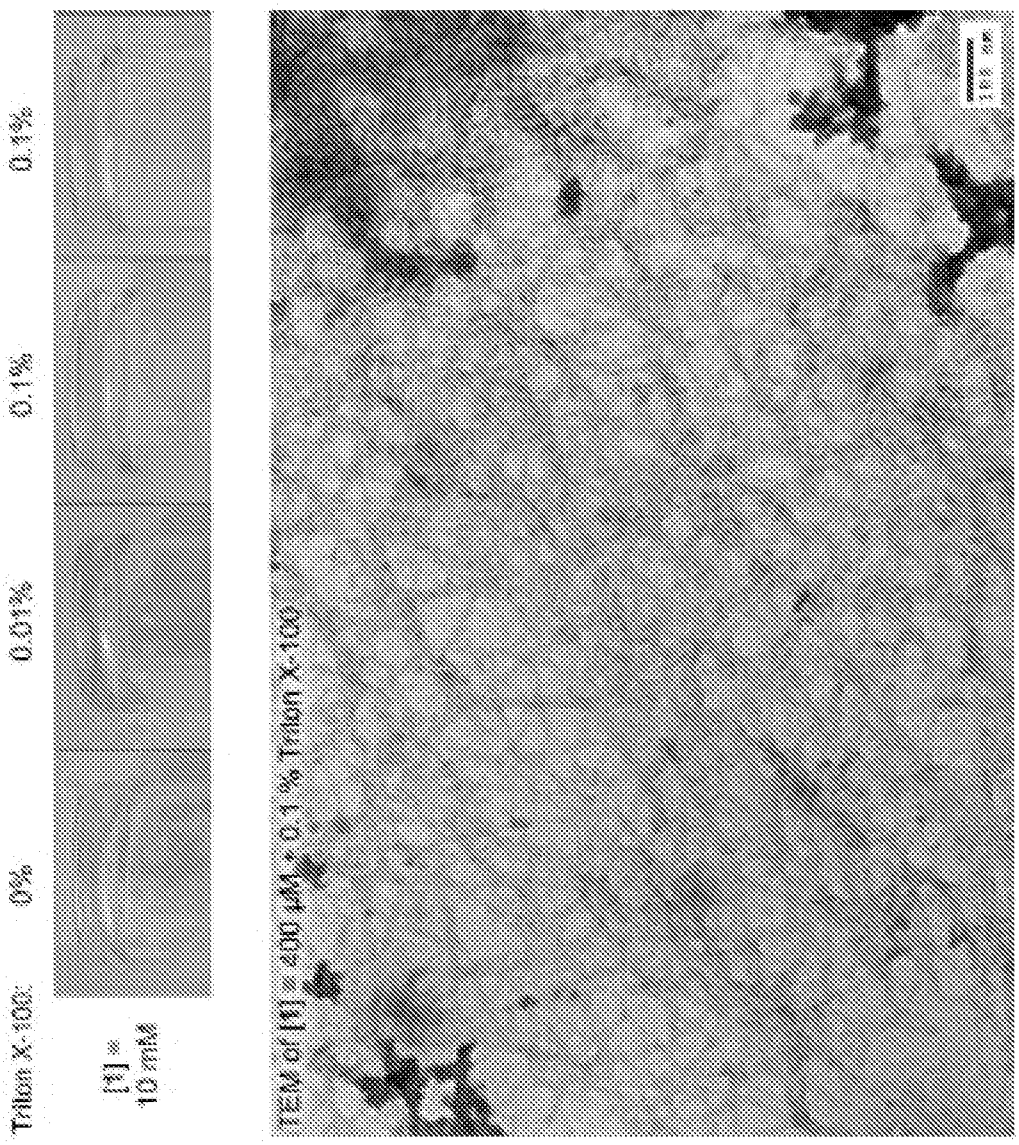
Added before hydrogel formation
Triton X-100:
0%
0.01%
0.1%
Draped onto formed hydrogel
0.1%
[T] = 10 mM
TEM of [T] = 400 μM + 0.1 % Triton X-100

Figure 14

Figure 15

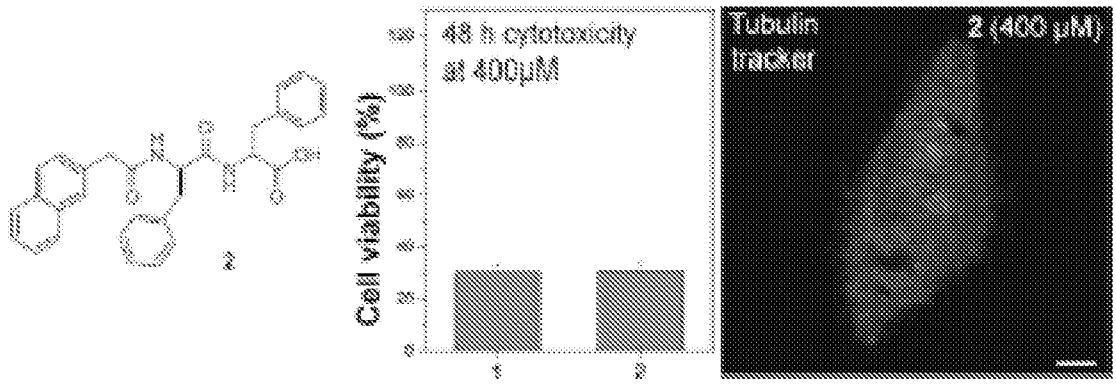
48 h cytotoxicity
at 400μM
Cell viability (%)
Tubulin
tracker
2 (400 μM)

Figure 16

Protein	Coverage (%)
BASP1	66.5
CCT2	63.4
TUBA4A	56.5
SERPINH1	54.4
TUBB2C	53.8
FKBP4	52.1
ATP5B	51.2
VIM	50.9
ENO1	50.4
TUFM	48.6
NUDC	48
PDIA3	47.4
G6PD	45.9
SSB	45.6
EIF4A1	45.3
EIF4A3	45.3
PSMC3	44.2
GPI	44.1
BZW1	43.9
DNAJA1	43.6
PSMD11	42.8
PDIA6	42.3
EIF3E	40.2
ATP5A1	40

Figure 17

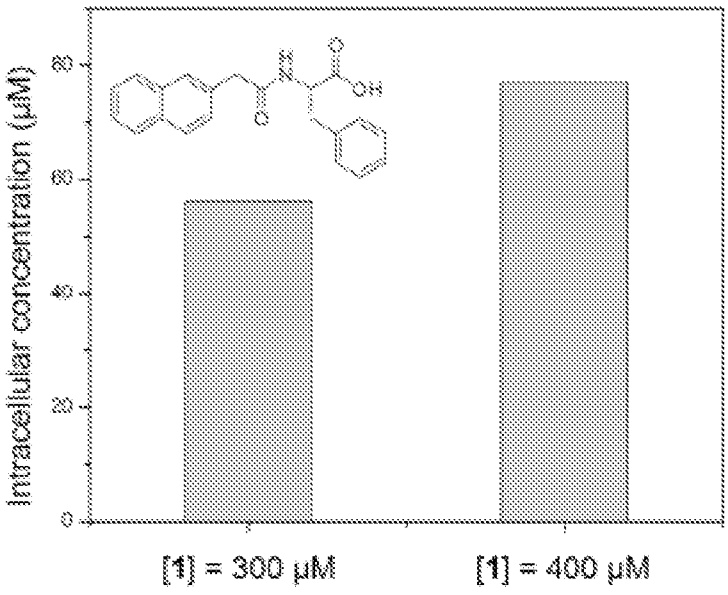

Figure 18

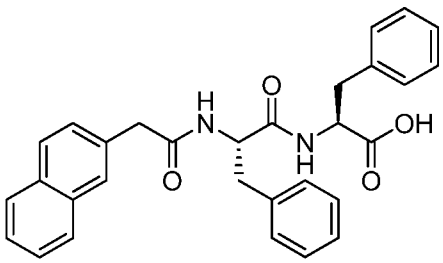

1

Figure 19

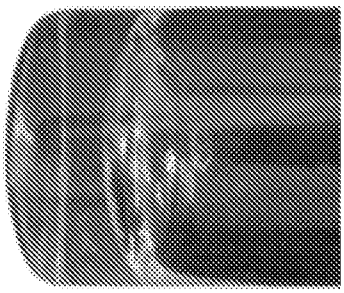

Figure 20

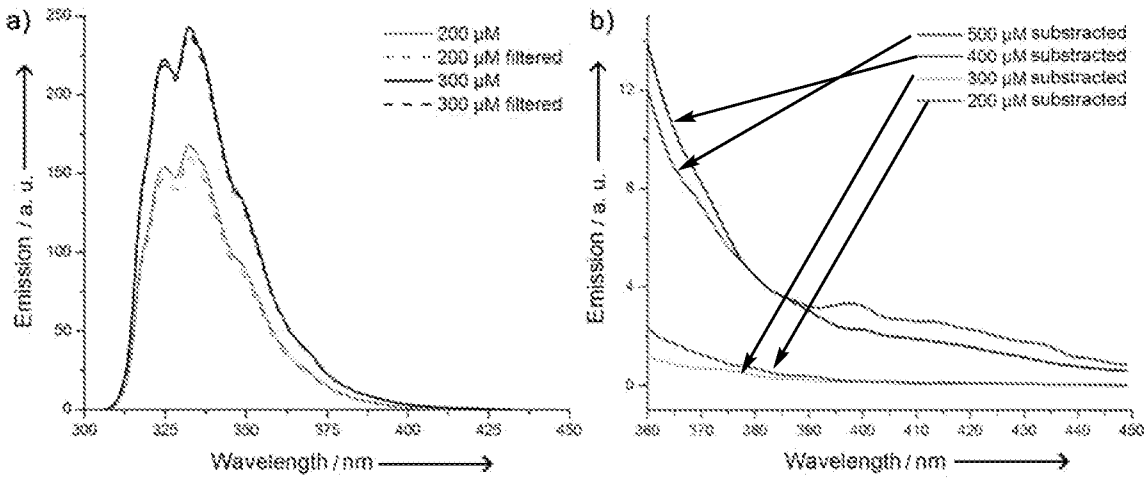

Figure 21

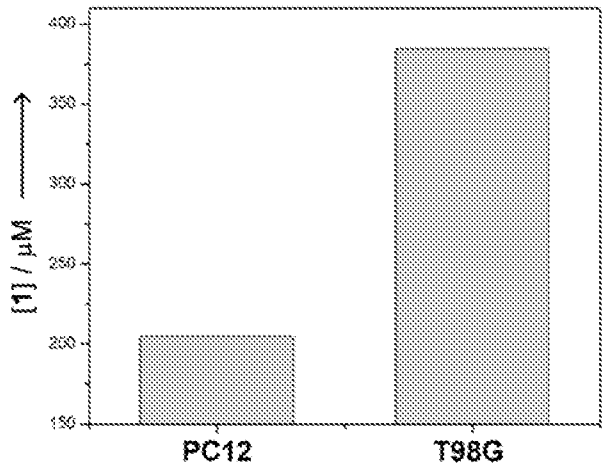

Figure 22

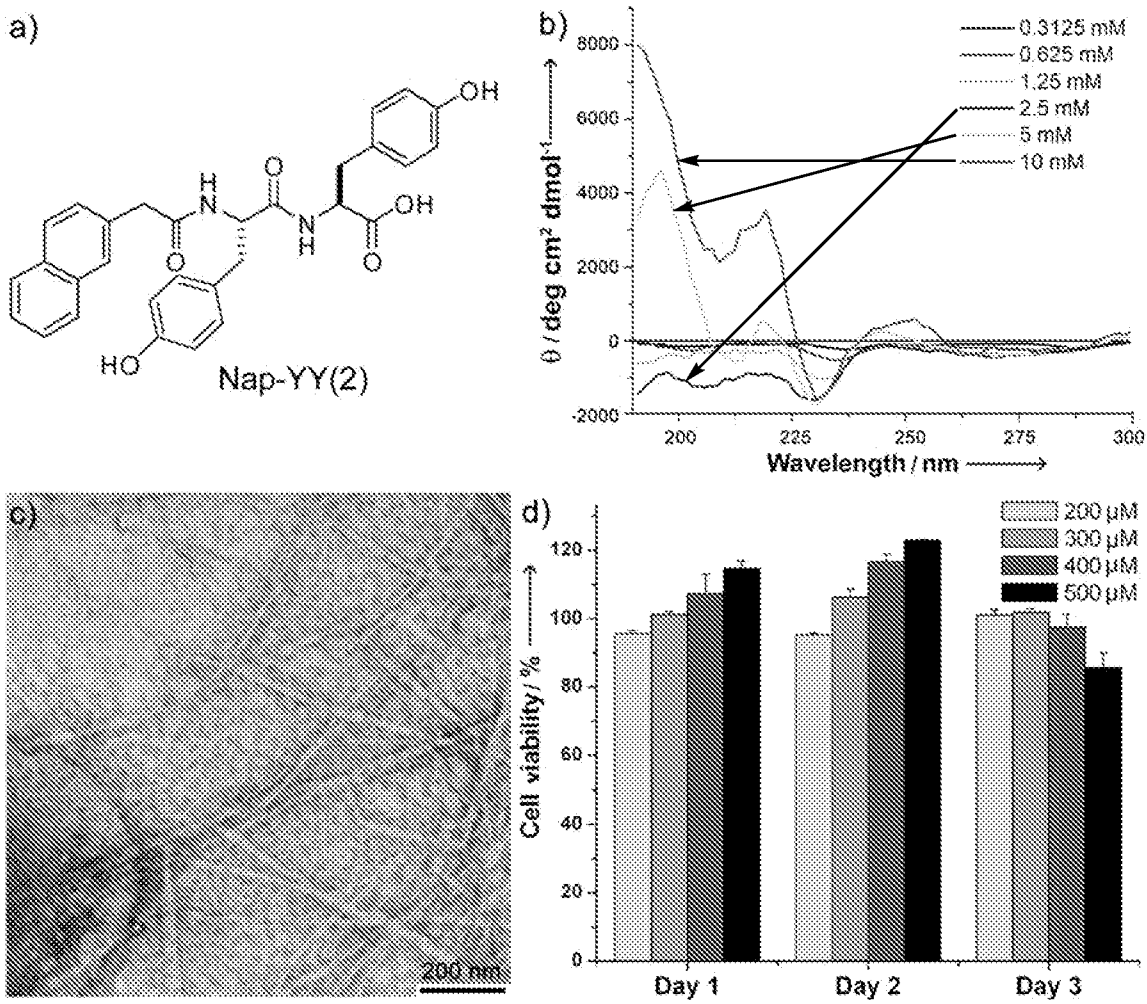

Figure 23

Initial concentration (μM)	Concentration after filtration(μM)[a]
200	190
300	251
400	336
500	329

Figure 24

Protein name	Total peptide #	Peptide	Peptide #	Reference	Protein coverage (%)
Tubulin, beta	135	KEVDEQMLNVQNKN	6	TUBB2C_IPI:IPI00007752.1	54.2
		KFWEVISDEHGIDPTGTYHGDSDLQLERI	1		
		KGHYTEGAELVDSVLDVVRK	7		
		KGHYTEGAELVDSVLDVVRKE	1		
		KLTTPTYGDLNHLVSATMSGVTTCLRF	2		
		KNMMAACDPRH	2		
		KNSSYFVEWIPNNVKT	7		
		KRISEQFTAMFRR	1		
		RALTVPELTQQMFDAKN	5		
		RAVLVDLEPGTMDSVRS	3		
		REIVHLQAGQCNQIGAKF	2		
		RIMNTFSVVPSPKV	6		
		RINVYYNEATGGKY	3		
		RISEQFTAMFRR	4		
		RLHFFMPGFAPLTSRG	8		
		RMSMKEVDEQMLNVQNKN	4		
		RSGPFGQIFRPDNFVFGQSGAGNNWAKG	4		
		RYLTVAAVFRG	2		
		KFWEVISDEHGIDPTGTYHGDSDLQLDRI	1	TUBB_IPI:IPI00011654.2	23.2
		KMAVTFIGNSTAIQELFKR	12		
		RAILVDLEPGTMDSVRS	6		
		RALTVPELTQQVFDAKN	8		
		REIVHIQAGQCGNQIGAKF	2		
		RISVYYNEATGGKY	2		
		KFWEVISDEHGIDPAGGYVGDSALQLERI	1	TUBB6_IPI:IPI00641706.1	18.8
		KLTTPTYGDLNHLVSATMSGVTTSLRF	3		
		RALTVPELTQQMFDARN	1		
		RISEQFSAMFRR	1		
		KEVDEQMLAIQSKN	2	TUBB3_IPI:IPI00013683.2	16.7
		KLATPTYGDLNHLVSATMSGVTTSLRF	1		
		KMSSTFIGNSTAIQELFKR	1		
		RISVYYNEASSHKY	1		
		RYLTVATVFRG	1		

Figure 24 (continued)

		KIREEYPDRI	1	TUBB1_IPI:IPI00006510.1	6.4
		KLAVNMVPFPRL	5		
		RFPGQLNADLRK	7		
		RFPGQLNADLRKL	2		
		RKLAVNMVPFPRL	1		
		RAALVDLEPGTMDSVRS	2	TUBB6_IPI:IPI00646779.2	9.2
		RSGPFGQLFRPDNFIFGQTGAGNNWAKG	1		
		RALTVPELTQQMFDSKN	1	TUBB2A_IPI:IPI00013475.1	8.8
		R.MNTFSVMPSPKV	2		
		RINVYYNEAAGNKY	1		
		KGHYTEGAELVDAVLDVVRK	1	TUBB4_IPI:IPI00023598.2	4.1
Tubulin, alpha	83	KAYHEQLSVAEITNACFEPANQMVKC	3	TUBA4A_IPI:IPI00007750.1	56.9
		KDVNAAIAAIKT	2		
		KEIIDPVLDRI	1		
		KFDLMYAKR	3		
		KRAFVHWYVGEGMEEGEFSEAREE	1		
		KTIGGGDDSFTTFFCETGAGKH	1		
		KVGINYQPPTVVPGGDLAKV	6		
		RAFVHWYVGEGMEEGEFSEARE	5		
		RAVCMLSNTTAIAEAWARL	4		
		RAVFVDLEPTVIDEIRN	3		
		REDMAALEKD	1		
		RFDGALNVDLTEFQTNLVPYPRI	1		
		RGHYTIGKE	1		
		RIHFPLATYAPVISAEKA	11		
		RLDHKFDLMYAKR	3		
		RLISQIVSSITASLRF	3		
		RLSVDYGKK	1		
		RLSVDYGKKS	2		
		RNLDIERPTYTNLNRL	2		
		RQLFHPEQLITGKE	5		
		RQLFHPEQLITGKEDAANNYARG	2		
		RRNLDIERPTYTNLNRL	1		
		KAYHEQLTVAEITNACFEPANQMVKC	1	TUBA1C_IPI:IPI00166768.3	23.9
		KDVNAAIATIKT	2		
		KEIIDLVLDRI	1		
		KTIGGGDDSFNTFFSETGAGKH	4		

Figure 24 (continued)

		RAVFVDLEPTVIDEVRT	4		
		KDYEEVGVDSVEGEGEEEGEEY	3	TUBA1A_IPI:IPI00180675.4	6.4
		REDMAALEKDYEEVGVDSVEGEGEEEGEEY	2		
		KDYEEVGADSADGEDEGEEY	1	TUBA1C_IPI:IPI00218343.4	6
		REDMAALEKDYEEVGADSADGEDEGEEY	1		
		RLIGQIVSSITASLRF	1	TUBA3D_IPI:IPI00179709.4	3.1
		RQIFHPEQLITGKE	1	TUBA4B_IPI:IPI00017454.4	5
T-complex protein1 subunit beta	50	KEAVAMESYAKA	3	CCT2_IPI:IPI00297779.7	63.4
		KILIANTGMDTDKIKI	1		
		KKIHPQTIIAGWRE	1		
		KKLGGSLADSYLDEGFLLDKK	1		
		KKLGGSLADSYLDEGFLLDKKI	1		
		KLAVEAVLRL	1		
		KLGGSLADSYLDEGFLLDKK	1		
		KLGGSLADSYLDEGFLLDKKI	4		
		KLIEEVMIGEDKL	1		
		KNIGVDNPAAKV	1		
		KVAEIEHAEKEKM	1		
		KVLVDMSRV	1		
		RAAHSEGNTTAGLDMRE	3		
		RDASLMVTNDGATILKN	4		
		REAESLIAKK	1		
		REALLSSAVDHGSDEVKF	1		
		REGTIGDMAILGITESFQVKR	4		
		RGATQQILDEAERS	1		
		RLALVTGGEIASTFDHPELVKL	2		
		RLKGSGNLEAIHIIKK	1		
		RLTSFIGAIAIGDLVKS	1		
		RMLPTIIADNAGYDSADLVAQLRA	4		
		RQDLMNIAGTTLSSKL	4		
		RQLIYNYPEQLFGAAGVMAIEHADFAGVERL	3		
		RQVLLSAAEAAEVILRV	2		
		RVQDDEVGDGTTSVTVLAAELLRE	2		
Actin, beta	44	KDLYANTVLSGGTTMYPGIADRM	13	ACTB_IPI:IPI00021439.1	36.5
		KLCYVALDFEQEMATAASSSSLEKS	1		
		KQEYDESGPSIVHRK	4		
		KYPIEHGIVTNWDDMEKI	2		

Figure 24 (continued)

		RDIKEKLCYVALDFEQEMATAASSSSLEKS	1		
		RGYSFTTTAERE	3		
		RKDLYANTVLSGGTTMYPGIADRM	6		
		RTTGIVMDSGDGVTHTVPIYEGYALPHAILRL	8		
		RVAPEEHPVLLTEAPLNPKA	6		
Vimentin	37	KFADLSEAANRN	1	VIM_IPI:IPI00418471.6	51.1
		KILLAELEQLKG	1		
		KILLAELEQLKGQGKS	1		
		KLQEEMLQRE	2		
		KLQEEMLQREEAENTLQSFRQ	1		
		KVELQELNDRF	1		
		RDGQVINETSQHHDDLE	1		
		RDNLAEDIMRL	1		
		REKLQEEMLQRE	1		
		REKLQEEMLQREEAENTLQSFRQ	1		
		REMEENFAVEAANYQDTIGRL	3		
		RETNLDSLPLVDTHSKR	2		
		RFANYIDKV	1		
		RISLPLPNFSSLNLRE	2		
		RKVESLQEEIAFLKK	2		
		RKVESLQEEIAFLKKL	1		
		RLGDLYEEEMRE	2		
		RLLQDSVDFSLADAINTEFKN	3		
		RLQDEIQNMKE	1		
		RLQDEIQNMKEEMARH	1		
		RQVDQLTNDKA	1		
		RRQVDQLTNDKA	1		
		RSLYASSPGGVYATRS	1		
		RTNEKVELQELNDRF	2		
		RTYSLGSALRPSTSRS	1		
		RVEVERDNLAEDIMRL	2		
Protein Disulfide Isomerase Family A, Member 3	35	KDASIVGFFDDSFSEAHSEFLKA	1	PDIA3_IPI:IPI00025252.1	47.5
		KDLLIAYYDVDYEKN	2		
		KDPNIVIAKM	1		
		KFEDKTVAYTEQKM	1		
		KFVMQEEFSRD	2		
		KGSNYWRN	1		
		KIFRDGEEAGAYDGPRT	2		
		KLNFAVASRK	2		
		KLSKDPNIVIAKM	1		

Figure 24 (continued)

		KMDATANDVPSPYEVRG	3		
		KQAGPASVPLRT	1		
		KRLAPEYEAAATRL	1		
		KSEPIPESNDGPVKV	1		
		KTFSHELSDFGLESTAGEIPVVAIRT	1		
		KTVAYTEQKM	1		
		KYGVSGYPTLKI	1		
		RDGEEAGAYDGPRT	2		
		REATNPPVIQEEKPKK	1		
		RELSDFISYLQRE	1		
		RFLQDYFDGNLKR	1		
		RFLQDYFDGNLKRY	1		
		RGFPTIYFSPANKK	2		
		RKTFSHELSDFGLESTAGEIPVVAIRT	1		
		RLAPEYEAAATRL	2		
		RTADGIVSHLKK	1		
		RTADGIVSHLKKQ	1		
Enolase 1, (alpha)	35	KAGYTDKVVIGMDVAASEFFRS	1	ENO1_IPI:IPI00465248.5	50.7
		KDATNVGDEGGFAPNILENKE	2		
		KDATNVGDEGGFAPNILENKEGLELLKT	1		
		KDYPVVSIEDPFDQDDWGAWQKF	2		
		KFTASAGIQVVGDDLTVTNPKR	3		
		KLAMQEFMILPVGAANFRE	10		
		KLAQANGWGVMVSHRS	1		
		KSFIKDYPVVSIEDPFDQDDWGAWQKF	1		
		KTIAPALVSKK	1		
		KVVIGMDVAASEFFRS	3		
		RGNPTVEVDLFTSKG	1		
		RHIADLAGNSEVILPVPAFNVINGGSHAGNKL	1		
		RIEEELGSKA	3		
		RIGAEVYHNLKN	1		
		RSGKYDLDFKS	1		
		RSGKYDLDFKSPDDPSRY	1		
		RYISPDQLADLYKS	2		
FK506 binding protein 4	34	KAEASSGDHPTDTEMKEEQKS	2	FKBP4_IPI:IPI00219005.3	52.7
		KATESGAQSAPLPMEGVDISPKQ	4		
		KAWDIAIATMKV	2		
		KDKFSFDLGKGEVIKA	1		

Figure 24 (continued)

		KESWEMNSEEKL	1		
		KFDSSLDRK	1		
		KFDSSLDRKD	1		
		KGEDLTEEEDGGIIRR	1		
		KGEHSIVYLKPSYAFGSVGKE	2		
		KIVSWLEYESSFSNEEAQKA	1		
		KKIVSWLEYESSFSNEEAQKA	1		
		KLEQSTIVKE	1		
		KLYANMFERL	2		
		KVLQLYPNNKA	2		
		REGTGTEMPMIGDRV	3		
		RFEIGEGENLDLPYGLERA	3		
		RGEAHLAVNDFELARA	1		
		RGEGYAKPNEGAIVEVALEGYYKD	1		
		RGEGYAKPNEGAIVEVALEGYYKDKL	1		
		RRGEAHLAVNDFELARA	1		
		RVFVHYTGWLLDGTKF	2		
Glucose-6-phosphate dehydrogenase	31	KEMVQNLMVLRF	2	G6PD_IPI:IPI00216008.4	45.8
		KGYLDDPTVPRG	1		
		KKPGMFFNPEESELDLTYGNRY	3		
		KLKLEDFFARN	1		
		KLPDAYERL	1		
		KRNELVIRV	1		
		RDGLLPENTFIVGYARS	2		
		REELFQGDAFHQSDTHIFIIMGASGDLAKK	1		
		RGGYFDEFGIIRG	1		
		RGPTEADELMKR	1		
		RGPTEADELMKRV	1		
		RGSTTATFAAVVLYVENERW	2		
		RIFGPIWNRD	1		
		RIIVEKPFGRD	1		
		RLFYLALPPTVYEAVTKN	2		
		RLNSHMNALHLGSQANRL	1		
		RLSNHISSLFRE	2		
		RLTVADIRK	1		
		RNSYVAGQYDDAASYQRL	3		
		RVGFQYEGTYKW	1		
		RVQPNEAVYTKM	1		
		RWDGVPFILRC	1		
Serpin peptidase inhibitor, clade H	30	KAATLAERS	1	SERPINH1_IPI:IPI00032140.4	54.8

Figure 24 (continued)

		KAVAISLPKG	1		
		KAVLSAEQLRD	1		
		KGVVEVTHDLQKH	2		
		KHLAGLGLTEAIDKN	2		
		KHLAGLGLTEAIDKNKA	2		
		KKAVAISLPKG	1		
		KKPAAAAAPGTAEKL	2		
		KLFYADHPFIFLVRD	1		
		KLQIVEMPLAHKL	2		
		KLSSLIILMPHHVEPLERL	2		
		RDEEVHAGLGELLRS	2		
		RDTQSGSLLFIGRL	1		
		RLYGPSSVSFADDFVRS	1		
		RSAGLAFSLYQAMAKD	1		
		RSALQSINEWAAQTTDGKL	2		
		RSALQSINEWAAQTTDGKLPEVTKD	1		
		RSALQSINEWAAQTTDGKLPEVTKDVERT	1		
		RSYTVGVMMMHRT	1		
		RTDGALLVNAMFFKPHWDEKF	1		
		RTGLYNYYDDEKE	1		
		RTGLYNYYDDEKEKL	1		
Eukaryotic translation elongation factor 1 alpha 2	29	KEGNASGVSLLEALDTILPPTRPTDKPLRL	1	EEF1A2_IPI:IPI00014424.1	30.2
		KEVSAYIKK	1		
		KFEKEAAEMGKG	2		
		KIGGIGTVPVGRV	3		
		KQLIVGVNKM	2		
		KSTTTGHLIYKC	3		
		KSVEMHHEALSEALPGDNVGFNVKN	1		
		KTHINIVVIGHVDSGKS	8		
		KYAWVLDKL	3		
		REHALLAYTLGVKQ	4		
		RQTVAVGVIKN	1		
Eukaryotic translation initiation factor 4A1	27	KATQALVLAPTRE	1	EIF4A1_IPI:IPI00025491.1	45.6
		KDQIYDIFQKL	1		
		KEELTLEGIRQ	1		
		KGVAINMVTEEDKRT	1		
		KGYDVIAQAQSGTGKT	1		
		KKEELTLEGIRQ	1		

Figure 24 (continued)

		KLNSNTQVVLLSATMPSDVLEVTKK	2		
		KLNSNTQVVLLSATMPSDVLEVTKKF	1		
		KLQMEAPHIIVGTPGRV	2		
		KMFVLDEADEMLSRG	3		
		RDFTVSAMHGDMDQKE	1		
		RELAQQIQKV	1		
		RENYIHRI	1		
		RGFKDQIYDIFQKL	1		
		RGIDVQQVSLVINYDLPTNRE	1		
		RKGVAINMVTEEDKRT	2		
		RQFYINVERE	2		
		RVFDMLNRR	3		
		RVLITTDLLARG	1		
Kappa-actin	26	KDLYANTVLSGGSTMYPGIADRM	1	ACTBL2_IPI:IPI00003269.1	25
		KIIAPPERKY	1		
		RDLTDYLMKI	4		
		RHQGVMVGMGQKD	11		
		RSYELPDGQVITIGNERF	8		
		RTTGIVMDSGDGVTHIVPIYEGYALPHAILRL	1		
Glucose-6-phosphate isomerase	25	KEFGIDPQNMFEFWDWVGGRY	2	GPI_IPI:IPI00027497.5	45
		KEWFLQAAKD	1		
		KHFVALSTNTTKV	2		
		KILLANFLAQTEALMRG	3		
		KLTPFMLGALVAMYEHKI	1		
		KNLVTEDVMRM	1		
		KNLVTEDVMRMLVDLAKS	1		
		KSPEDLERL	1		
		KTFTTQETITNAETAKE	1		
		KTITDVINIGIGGSDLGPLMVTEALKPYSSGGPRV	1		
		KTLAQLNPESSLFIIASKT	2		
		KVFEGNRPTNSIVFTKL	1		
		KVKEFGIDPQNMFEFWDWVGGRY	1		
		RFAAYFQQGDMESNGKY	2		
		RMLVDLAKS	1		
		RSNTPILVDGKD	1		
		RSNTPILVDGKDVMPEVNKV	1		
		RVDHQTGPIVWGEPGTNGQHAFYQLIHQGTKM	1		
		RVWYVSNIDGTHIAKT	1		

Figure 24 (continued)

Tu translation elongation factor, mitochondrial	24	KADAVQDSEMVELVELEIRE	4	TUFM_IPI:IPI00027107.5	48.6
		KELAMPGEDLKF	1		
		KILAEGGGAKF	1		
		KKYEEIDNAPEERA	1		
		KLLDAVDTYIPVPARD	1		
		KTTLTAAITKI	1		
		KVEAQVYILSKE	1		
		RAEAGDNLGALVRG	1		
		RDKPHVNVGTIGHVDHGKT	1		
		RDLEKPFLLPVEAVYSVPGRG	2		
		REHLLLARQ	1		
		RELLTEFGYKG	1		
		RGITINAAHVEYSTAARH	1		
		RGTVVTGTLERG	1		
		RIILPPEKELAMPGEDLKF	1		
		RQIGVEHVVVYVNKA	1		
		RTIGTGLVTNTLAMTEEEKN	3		
		RTVVTGIEMFHKS	1		
Actin, alpha	23	KAGFAGDDAPRA	3	ACTA2_IPI:IPI00008603.1	21
		KDSYVGDEAQSKR	2		
		KEITALAPSTMKI	6		
		KQEYDEAGPSIVHRK	3		
		KYPIEHGIITNWDDMEKI	5		
		RAVFPSIVGRPRH	1		
		KDSYVGHEAQSKR	1	ACTA2_IPI:IPI00927545.1	3.3
		KDLYANNVMSGGTTMYPGIADRM	1	ACTA1_IPI:IPI00021428.1	8.5
		KIWHHTFYNELRV	1		
Chaperonin containing TCP1, subunit 7 (eta)	22	KALEIIPRQ	1	CCT7_IPI:IPI00018465.1	34.1
		KATISNDGATILKL	1		
		KLLDVVHPAAKT	1		
		KLPIGDVATQYFADRD	1		
		KMVVDAVMMLDDLLQLKM	5		
		KNDSVVAGGGAIEMELSKY	2		
		KQQLLIGAYAKA	1		
		KSQDAEVGDGTTSVTLLAAEFLKQ	2		
		KTFSYAGFEMQPKK	2		
		KVQGGALEDSQLVAGVAFKK	2		
		RGGAEQFMEETERS	2		
		RSTVDAPTAAGRG	1		
		RVHTVEDYQAIVDAEWNILYDKL	1		

Figure 24 (continued)

		EKI			
Integrin-linked kinase	22	KGIEILTDMSRPVELSDRE	3	ILK-2_IPI:IPI00302927.6	33.8
		KGIEILTDMSRPVELSDRETLLNSATTSLNSKV	1		
		KLVIEEAERS	1		
		KMIQDGKGDVTITNDGATILKQ	2		
		KTDMDNQIVVSDYAQMDRV	4		
		KVIDPATATSVDLRD	2		
		KVSNSGITRV	2		
		KVVSQYSSLLSPMSVNAVMKV	2		
		RAFADAMEVIPSTLAENAGLNPISTVTELRN	2		
		RALIAGGGAPEIELALRL	1		
		RAYILNLVKQ	1		
		RDALSDLALHFLNKM	1		
Phosphoglycerate dehydrogenase	22	KFMGTELNGKT	1	PHGDH_IPI:IPI00011200.5	31
		KILQDGGLQVVEKQ	1		
		KQADVNLVNAKL	1		
		KQHVTEAFQFHF	2		
		KTLGILGLGRI	1		
		KVTADVINAAEKL	2		
		RAGTGVDNVDLEAATRK	2		
		RALQSGQCAGAALDVFTEEPPRDRA	1		
		RCGEEIAVQFVDMVKG	1		
		RDLPLLLFRT	1		
		RGGIVDEGALLRA	2		
		RQIPQATASMKD	1		
		RTQTSDPAMLPTMIGLLAEAGVRL	6		
Sjogren syndrome antigen B (autoantigen La)	21	KDANNGNLQLRN	1	SSB_IPI:IPI00009032.1	45.6
		KEVTWEVLEGEVEKE	1		
		KGFPTDATLDDIKEWLEDKG	1		
		KGFPTDATLDDIKEWLEDKGQVLNIQMRR	1		
		KGQVLNIQMRR	1		
		KGSIFVVFDSIESAKK	1		
		KIIEDQQESLNKW	2		
		KKFVETPGQKY	1		
		KLDEGWVPLEIMIKF	2		
		KLEEDAEMKS	1		
		KQKLEEDAEMKS	1		
		KSKAELMEISEDKTKI	1		
		KYKETDLLILFKD	1		

Figure 24 (continued)

		KYKETDLLILFKDDYFAKK	1		
		REDLHILFSNHGEIKW	1		
		RLTTDFNVIVEALSKS	1		
		RNKEVTWEVLEGEVEKE	1		
		RSPSKPLPEVTDEYKNDVKN	2		
nudC nuclear distribution protein	21	KDAENHEAQLKN	1	NUDC_IPI:IPI00550746.4	48
		KDMVVDIQRR	1		
		KELTDEEAERL	1		
		KELTDEEAERLQLEIDQKK	1		
		KFMDQHPEMDFSKA	1		
		KGQPAIIDGELYNEVKV	1		
		KKDAENHEAQLKN	1		
		KLITQTFSHHNQLAQKT	1		
		KLKPNLGNGADLPNYRW	3		
		KLSDLDSETRS	1		
		KSMGLPTSDEQKK	2		
		KTDFFIGGEEGMAEKL	2		
		KVEESSWLIEDGKV	1		
		KVVTVHLEKI	1		
		RKTDFFIGGEEGMAEKL	1		
		RLQLEIDQKK	1		
		RLVSSDPEINTKK	1		
Inosine 5'-monophosphate dehydrogenase 2	21	KALALGASTVMMGSLLAATTEAPGEYFFSDGIRL	1	IMPDH2_IPI:IPI00291510.3	37.7
		KDKYPNLQVIGGNVVTAAQAKN	2		
		KGKLPIVNEDDELVAIIART	2		
		KNLIDAGVDALRV	2		
		KREDLVVAPAGITLKE	2		
		KVAQGVSGAVQDKG	2		
		KVSEYARR	1		
		KYEQGFITDPVVLSPKD	1		
		REDLVVAPAGITLKE	1		
		RFGVPVIADGGIQNVGHIAKA	1		
		RGMGSLDAMDKH	1		
		RLVGIISSRD	1		
		RRFGVPVIADGGIQNVGHIAKA	1		
		RTSSAQVEGGVHSLHSYEKR	2		
		RYFSEADKIKV	1		
Brain abundant, membrane attached signal protein 1[a]	21	KAEGAATEEEGTPKE	3	BASP1_IPI:IPI00299024.9	66.5
		KAEGAATEEEGTPKESEPQAAAEPAEAKE	1		
		KAEPEKTEGAAEAKA	1		
		KAEPPKAPEQEQAAPGPAAGGE	5		

Figure 24 (continued)

		APKA			
		KAPEQEQAAPGPAAGGEAPKA	1		
		KAQGPAASAEEPKPVEAPAANSDQTVTVKE	4		
		KETPAATEAPSSTPKA	1		
		KGYNVNDEKA	1		
		KKAEGAATEEEGTPKE	1		
		KKTEAPAAPAAQETKS	1		
		KSDGAPASDSKPGSSEAAPSSKE	2		
Eukaryotic translation elongation factor 1 alpha 1	21	KDGNASGTTLLEALDCILPPTRPTDKPLRL	2	EEF1A1_IPI:IPI00025447.8	23.8
		KEVSTYIKK	1		
		KSGDAAIVDMVPGKPMCVESFSDYPPLGRF	5		
		KYYVTIIDAPGHRD	4		
		RVETGVLKPGMVVTFAPVNVTTEVKS	8		
		RYEEIVKE	1		
ATP synthase, H+ transporting, mitochondrial F1 complex, alpha subunit 1	20	KAVDSLVPIGRG	1	ATP5A1_IPI:IPI00440493.2	40
		KEIVTNFLAGFEA	1		
		KFENAFLSHVVSQHQALLGTIRA	1		
		KGIRPAINVGLSVSRV	1		
		KGMSLNLEPDNVGVVVFGNDKL	2		
		KHALIIYDDLSKQ	1		
		KQGQYSPMAIEEQVAVIYAGVRG	3		
		KTGTAEMSSILEERI	1		
		KTSIAIDTIINQKR	1		
		REAYPGDVFYLHSRL	1		
		REVAAFAQFGSDLDAATQQLLSRG	2		
		RILGADTSVDLEETGRV	2		
		RNVQAEEMVEFSSGLKG	1		
		RVLSIGDGIARV	1		
		RVVDALGNAIDGKG	1		
Fascin homolog 1, actin-bundling protein	20	KKNGQLAASVETAGDSELFLMKL	1	FSCN1_IPI:IPI00163187.1	37.5
		KLINRPIIVFRG	1		
		KNGQLAASVETAGDSELFLMKL	1		
		KVNASASSLKK	1		
		KVNASASSLKKK	1		
		KYLTAEAFGFKV	1		
		KYWTLTATGGVQSTASSKN	1		
		RDVPWGVDSLITLAFQDQRY	1		
		RFLIVAHDDGRW	2		

Figure 24 (continued)

		RKVTGTLDANRSSYDVFQLEFNDGAYNIKD	1		
		RLVARPEPATGYTLEFRS	2		
		RQGMDLSANQDEETDQETFQLEIDRD	1		
		RQGMDLSANQDEETDQETFQLEIDRDTKK	2		
		RSSYDVFQLEFNDGAYNIKD	2		
		RWSLQSEAHRR	1		
		RYSVQTADHRF	1		
Eukaryotic translation initiation factor 4A3	20	KEQIYDVYRY	1	EIF4A3_IPI:IPI00009328.4	45.3
		KFMTDPIRI	1		
		KGRDVIAQSQSGTGKT	2		
		KLDYGQHVVAGTPGRV	2		
		KMLVLDEADEMLNKG	1		
		KRDELTLEGIKQ	1		
		KRKVDWLTEKM	1		
		RDIEQYYSTQIDEMPMNVADLI	1		
		RDVIAQSQSGTGKT	1		
		REANFTVSSMHGDMPQKE	1		
		RELAVQIQKG	1		
		RETQALILAPTRE	1		
		RGIYAYGFEKPSAIQQRA	2		
		RGLDVPQVSLIINYDLPNNRE	1		
		RKLDYGQHVVAGTPGRV	1		
		RLLKEEDMTKV	1		
		RVLISTDVWARG	1		

INTERNATIONAL SEARCH REPORT

International application No.
PCT/US14/21129

A. CLASSIFICATION OF SUBJECT MATTER
IPC(8) - A61K 31/513, 31/52 (2014.01)
USPC - 514/21.9; 530/330
According to International Patent Classification (IPC) or to both national classification and IPC

B. FIELDS SEARCHED

Minimum documentation searched (classification system followed by classification symbols)
IPC(8): A61K 31/513, 31/52; C07K 5/107 (2014.01)
USPC: 514/21.9, 19.3; 530/330

Documentation searched other than minimum documentation to the extent that such documents are included in the fields searched

Electronic data base consulted during the international search (name of data base and, where practicable, search terms used)
MicroPatent (US-G, US-A, EP-A, EP-B, WO, JP-bib, DE-C,B, DE-A, DE-T, DE-U, GB-A, FR-A); ProQuest; Scifinder; Google/Google Scholar; KEYWORDS: hydrophobic, small, molecules, self-assembly, microtubules, cancer, aberrant, proteins, fibrillar, inhibition, carcinoma, tumor, heterodimer, tubulin

C. DOCUMENTS CONSIDERED TO BE RELEVANT

Category*	Citation of document, with indication, where appropriate, of the relevant passages	Relevant to claim No.
X -- Y	US 2012/0142616 A1 (GAO, Y et al.) 07 June 2012; formula I; paragraphs [0005], [0015], [0050], [0116] and [0141]	1-6, 7/1-6 ---------- 8/1-6, 9/8/1-6, 10/8/1-6, 11/8/1-6, 26/1-6, 27/1-6
Y	WO 2012/166706 A2 (XU, B) 06 December 2012; formula I; page 1, lines 22-30; page 2, lines 1-4	8/1-6, 9/8/1-6, 10/8/1-6, 11/8/1-6, 26/1-6, 27/1-6
A	WO 2012/166705 A2 (XU, B) 06 December 2012; entire document	1-6, 7/1-6, 8/1-6, 9/8/1-6, 10/8/1-6, 11/8/1-6, 26/1-6, 27/1-6

☐ Further documents are listed in the continuation of Box C. ☐

* Special categories of cited documents:
"A" document defining the general state of the art which is not considered to be of particular relevance
"E" earlier application or patent but published on or after the international filing date
"L" document which may throw doubts on priority claim(s) or which is cited to establish the publication date of another citation or other special reason (as specified)
"O" document referring to an oral disclosure, use, exhibition or other means
"P" document published prior to the international filing date but later than the priority date claimed
"T" later document published after the international filing date or priority date and not in conflict with the application but cited to understand the principle or theory underlying the invention
"X" document of particular relevance; the claimed invention cannot be considered novel or cannot be considered to involve an inventive step when the document is taken alone
"Y" document of particular relevance; the claimed invention cannot be considered to involve an inventive step when the document is combined with one or more other such documents, such combination being obvious to a person skilled in the art
"&" document member of the same patent family

Date of the actual completion of the international search	Date of mailing of the international search report
19 May 2014 (19.05.2014)	30 MAY 2014
Name and mailing address of the ISA/US Mail Stop PCT, Attn: ISA/US, Commissioner for Patents P.O. Box 1450, Alexandria, Virginia 22313-1450 Facsimile No. 571-273-3201	Authorized officer: Shane Thomas PCT Helpdesk: 571-272-4300 PCT OSP: 571-272-7774

Form PCT/ISA/210 (second sheet) (July 2009)

INTERNATIONAL SEARCH REPORT

International application No.
PCT/US14/21129

Box No. II Observations where certain claims were found unsearchable (Continuation of item 2 of first sheet)

This international search report has not been established in respect of certain claims under Article 17(2)(a) for the following reasons:

1. ☐ Claims Nos.:
because they relate to subject matter not required to be searched by this Authority, namely:

2. ☐ Claims Nos.:
because they relate to parts of the international application that do not comply with the prescribed requirements to such an extent that no meaningful international search can be carried out, specifically:

3. ☒ Claims Nos.: 12-25
because they are dependent claims and are not drafted in accordance with the second and third sentences of Rule 6.4(a).

Box No. III Observations where unity of invention is lacking (Continuation of item 3 of first sheet)

This International Searching Authority found multiple inventions in this international application, as follows:

1. ☐ As all required additional search fees were timely paid by the applicant, this international search report covers all searchable claims.

2. ☐ As all searchable claims could be searched without effort justifying additional fees, this Authority did not invite payment of additional fees.

3. ☐ As only some of the required additional search fees were timely paid by the applicant, this international search report covers only those claims for which fees were paid, specifically claims Nos.:

4. ☐ No required additional search fees were timely paid by the applicant. Consequently, this international search report is restricted to the invention first mentioned in the claims; it is covered by claims Nos.:

Remark on Protest

☐ The additional search fees were accompanied by the applicant's protest and, where applicable, the payment of a protest fee.

☐ The additional search fees were accompanied by the applicant's protest but the applicable protest fee was not paid within the time limit specified in the invitation.

☐ No protest accompanied the payment of additional search fees.